Aggregation of self-assembling branched [*n*]rotaxanes†

David B. Amabilino,‡·[a] Masumi Asakawa,[b] Peter R. Ashton,[a] Roberto Ballardini,[c] Vincenzo Balzani,[d] Martin Bělohradský,[a] Alberto Credi,[d] Masahiro Higuchi,[b] Françisco M. Raymo,§·[a] Toshimi Shimizu,[b] J. Fraser Stoddart,*·§·[a] Margherita Venturi[d] and Kiyoshi Yase[b]

[a] *School of Chemistry, University of Birmingham, Edgbaston, Birmingham, UK B15 2TT*
[b] *National Institute of Materials and Chemical Research, 1-1 Higashi, Tsukuba, Ibaraki 305, Japan*
[c] *Istituto FRAE-CNR, via Gobetti 101, 40129 Bologna, Italy*
[d] *Dipartimento di Chimica "G. Ciamician" dell'Università, via Selmi 2, 40126 Bologna, Italy*

The so-called slippage methodology has been employed to self-assemble novel [2]-, [3]-, and [4]-rotaxanes incorporating, respectively, one, two, and three bis-*p*-phenylene-34-crown-10 macrocyclic components and a branched 'dumbbell' component, consisting of three arms containing bipyridinium units attached covalently to a 1,3,5-trisubstituted benzene central core and each bearing at its other end a substituted tetraarylmethane stopper. The absorption spectra, luminescence properties, and electrochemical behaviour of the branched component and its [2]-, [3]-, and [4]-rotaxanes have been investigated and discussed on the basis of the properties of their chromophoric and electroactive units. Charge- and energy-transfer processes between specific chromophoric units and the correlations between the unusual redox patterns of the various compounds have been evidenced and interpreted. The ^{1}H-NMR spectroscopic investigation of the 'free' triply-branched hexacationic core, containing three bipyridinium units, one in each arm and terminated by bulky hydrophobic tetraarylmethane-based stoppers revealed, in chloroform solution, the formation of aggregates—a phenomenon which has been modeled using force field calculations. In addition, the formation of a gel was observed after the slow liquid–liquid diffusion of hexane into a chloroform solution of the triply-branched compound. Field-emission scanning electron microscopic investigation of this gel revealed the presence of domains of regular size. Surface-pressure–area measurements demonstrated the formation of stable monolayers by the 'free' backbone and the rotaxanes at an air–water interface: two distinct aggregates are formed by each compound. Interestingly, for the rotaxanes, the measured limiting area per molecule of both aggregates increases with the number of macrocyclic components which are incorporated within the rotaxane molecule. Atomic force microscopic analyses of the monolayers transferred onto mica revealed significant differences in their shapes when the two distinct aggregates formed by the same compound at different pressures were compared. In particular, the section analyses of the monolayers showed nanosized domains possessing diameters ranging from approximately 10 to 56 nm.

Rotaxanes and polyrotaxanes (Fig. 1) are molecular compounds composed of a backbone incorporating thread-like units, encircled by one or more macrocyclic components.[2] Bulky groups termed stoppers are attached covalently to one or both ends of the thread-like units in order to prevent dethreading of the macrocyclic component. As a result, *mechanical bonds* are ultimately responsible for holding together such molecular assemblies. Most of the rotaxanes and polyrotaxanes reported in the literature so far incorporate a dumbbell-shaped backbone (Fig. 1a) composed of a thread-like unit having stoppers at both ends. However, recently, several investigators have explored the possibility of generating rotaxanes and polyrotaxanes incorporating backbones with different topologies. In particular, a number of side-chain polyrotaxanes of the type schematically shown in Fig. 1b and 1c have been synthesized by Born and Ritter,[3] employing cyclodextrins as the macrocyclic components. On the other hand, we have envisaged the possibility of synthesizing branched rotaxanes (Fig. 1d) with the ultimate goal of generating dendritic[4] polyrotaxanes. The backbones of these rotaxanes incorporate three thread-like units attached covalently to a central core and bearing at the other end a bulky stopper. Thus, when one, two, or all three thread-like units are encircled by a macrocyclic component, a [2]-, a [3]-, or a [4]-rotaxane, respectively, is obtained. By replacing the stoppers with appropriate branching points and attaching covalently a new generation of thread-like units encircled by a macrocyclic component to them, it should be possible, in principle, to con-

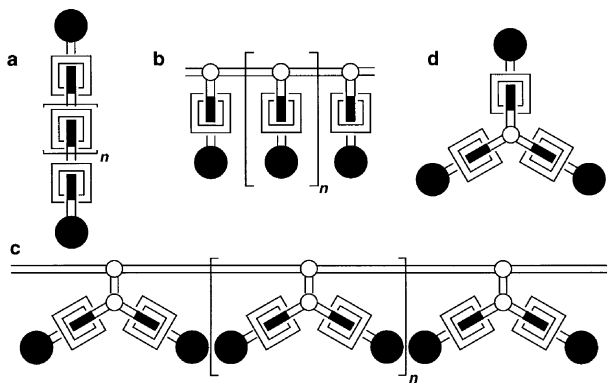

Fig. 1 Schematic representation of (a) main-chain, (b, c) side-chain, and (d) branched rotaxanes

* Fax: +1310 206 1843; E-mail: stoddart@chem.ucla.edu
† "Molecular Meccano," Part 36[1].
‡ Present address: Institut de Ciència de Materials e Barcelona (CSIC), Campus Universitari, 08193-Bellaterra, Spain.
§ Present address: Department of Chemistry and Biochemistry, University of California, Los Angeles, 405 Hilgard Avenue, Los Angeles, CA 90095-1569, USA.

struct dendritic structures generation after generation—namely, dendritic polyrotaxanes.

The synthetic strategy we have chosen to self-assemble branched rotaxanes, such as the one schematically depicted in Fig. 1d, is that of slippage.[5] This simple and appealing, and also efficient, approach to self-assembling rotaxanes involves the synthesis (*i*) of a π-electron rich hydroquinone-based macrocyclic polyether and (*ii*) of a π-electron deficient bipyridinium-based triply-branched backbone. The macrocycle must possess a cavity large enough to be able to slip over the stoppers of the backbone under the influence of an appropriate amount of thermal energy. The noncovalent bonding interactions between the recognition sites incorporated by design into the complementary components are responsible for driving the self-assembly process.[6] These interactions are (*i*) π–π stacking[7] between the complementary bipyridinium and hydroquinone aromatic units, as well as (*ii*) hydrogen bonding[8] between the polyether oxygen atoms and the hydrogen atoms in the α-positions with respect to the nitrogen atoms on the bipyridinium units. Here, we report: (*i*) the synthesis of a triply-branched bipyridinium-based hexakis(hexafluorophosphate) salt and the self-assembly of branched [2]-, [3]-, and [4]-rotaxanes incorporating the triply-branched backbone, encircled by one, two, or three bis-*p*-phenylene-34-crown-10 macrocyclic components, respectively, using the slippage approach; (*ii*) the formation of aggregates by the triply-branched bipyridinium-based hexakis(hexafluorophosphate) salt in chloroform solution and a computational analysis of this phenomenon; (*iii*) the ability of these molecules to form Langmuir films at air–water interfaces and their atomic force microscopic analyses; and (*iv*) the investigation of the charge- and energy-transfer processes occurring between the several chromophoric and electroactive units incorporated in these molecules, as well as their unusual redox properties.

Results and Discussion

Synthesis

The hexakis(hexafluorophosphate) salt $\mathbf{4}\cdot 6PF_6$ incorporates three bipyridinium recognition sites attached to a 1,3,5-trimethylenebenzene core and carries, at their termini, bis(4-*t*-butylphenyl)-4-methylphenylmethane-based stoppers. This compound was synthesized[5e] as illustrated in Scheme 1. Reaction of an excess of 4,4'-bipyridine with 1,3,5-tris(bromomethyl)benzene **1** in MeCN solution heated under reflux over4 d, followed by counter ion exchange, gave the tris(hexafluorophosphate) salt $\mathbf{2}\cdot 3PF_6$. Alkylation of $\mathbf{2}\cdot 3PF_6$ with the chloride **3** under ultrahigh pressure conditions in DMF at 40 °C over 48 h afforded the hexakis(hexafluorophosphate) salt $\mathbf{4}\cdot 6PF_6$ in a yield of 47% after counter ion exchange.

In previous work,[5a] we have demonstrated that the π-electron rich hydroquinone-based macrocyclic polyether, bis-*p*-phenylene-34-crown-10 (BPP34C10), possesses a cavity large enough to slip over the bis(4-*t*-butylphenyl)-4-methylphenylmethane-based stoppers at 50 °C in MeCN: these particular experimental conditions correspond to those we have employed[5] for the self-assembly of simple [2]rotaxanes by slippage. Thus, by heating an MeCN solution of the hexakis(hexafluorophosphate) salt $\mathbf{4}\cdot 6PF_6$ and 2 mol equivalents of BPP34C10 at 50 °C over 10 d, the [2]rotaxane $\mathbf{5}\cdot 6PF_6$, the [3]rotaxane $\mathbf{6}\cdot 6PF_6$, and [4]rotaxane $\mathbf{7}\cdot 6PF_6$ were self-assembled[5e] (Scheme 2) in yields of 46, 26, and 6%, respectively. When the reaction was repeated in the presence of 15 mol equivalents of BPP34C10 under otherwise identical conditions, corresponding yields were 19, 41, and 22%, respectively. Thus, despite the use of a very large excess of the macrocycle BPP34C10, the major product of the reaction is the [3]rotaxane $\mathbf{6}\cdot 6PF_6$ and not the 'fully-occupied' [4]rotaxane $\mathbf{7}\cdot 6PF_6$. Presumably, this result is a consequence of (*i*) the steric crowding around the central benzenoid core and (*ii*) the 'alongside' π–π stacking interactions between the hydroquinone rings of the two macrocyclic components already incorporated within the [3]rotaxane $\mathbf{6}\cdot 6PF_6$ and the 'free' bipyridinium unit. A combination of these two phenomena could result in a negative allosteric effect which enhances the free energy of activation associated with the slippage of the third macrocyclic component to afford $\mathbf{7}\cdot 6PF_6$.

Electrospray mass spectrometry

The hexakis(hexafluorophosphate) salt $\mathbf{4}\cdot 6PF_6$ and the rotaxanes $\mathbf{5}\cdot 6PF_6$, $\mathbf{6}\cdot 6PF_6$, and $\mathbf{7}\cdot 6PF_6$ were characterized

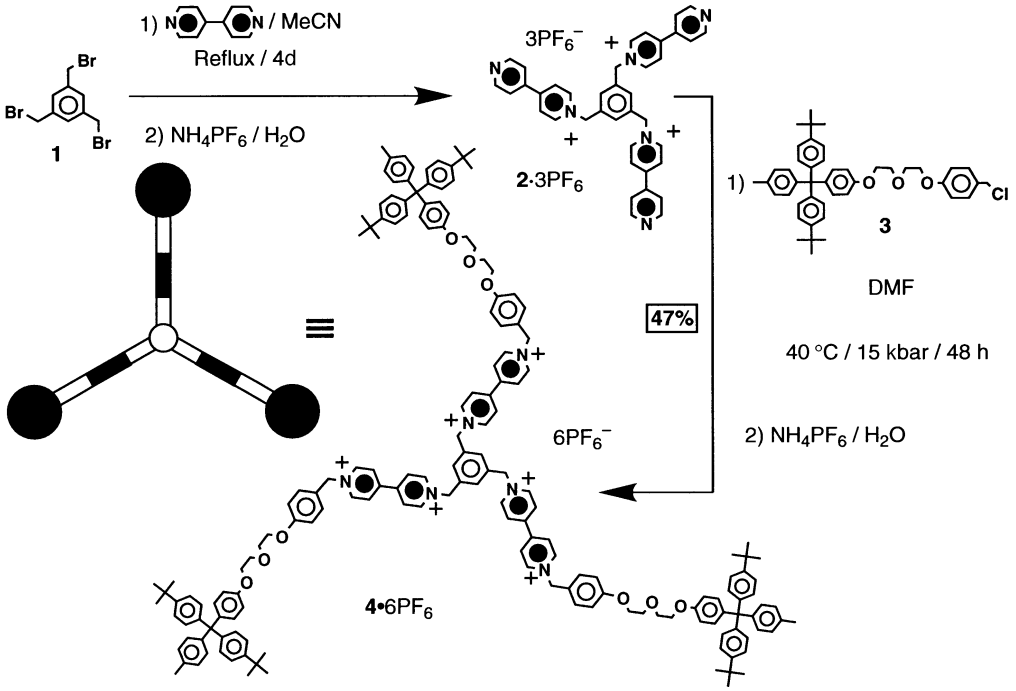

Scheme 1 Synthesis of the hexakis(hexafluorophosphate) salt $\mathbf{4}\cdot 6PF_6$

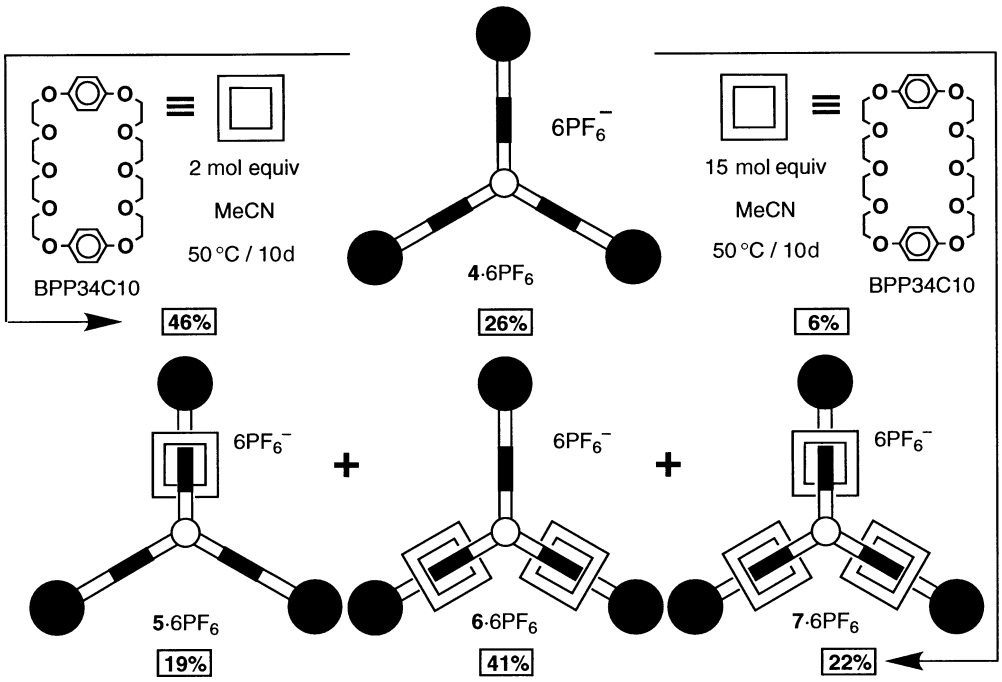

Scheme 2 Self-assembly of the [*n*]rotaxanes $5 \cdot 6PF_6$, $6 \cdot 6PF_6$ and $7 \cdot 6PF_6$ by slippage

(Table 1) by electrospray (ES) mass spectrometry. The ES mass spectra of all four compounds showed peaks at *m/z* values for $[M - 2PF_6]^{2+}$, corresponding to the loss of two hexafluorophosphate counter ions. In the case of the [3]rotaxane $6 \cdot 6PF_6$ and the [4]rotaxane $7 \cdot 6PF_6$, peaks for $[M - 3PF_6]^{3+}$ at *m/z* 1338 and 1517, respectively, corresponding to the loss of three hexafluorophosphate counter ions, were also observed. Furthermore, signals for $[2M - 3PF_6]^{3+}$ at *m/z* of 2106, 2464 and 2821, corresponding to the loss of three hexafluorophosphate counter ions from dimeric species, were observed[9] for $4 \cdot 6PF_6$, $5 \cdot 6PF_6$, and $6 \cdot 6PF_6$, respectively. Presumably, these dimers are formed as a result of intermolecular π–π stacking interactions.

^{1}H-NMR spectroscopy

The chemical shifts (δ) for the hydrogen atoms in the α- and β-positions with respect to the nitrogen atoms on the bipyridinium units, as well as for the hydrogen atoms attached to the hydroquinone rings of the macrocyclic polyether components in the rotaxanes $5 \cdot 6PF_6$, $6 \cdot 6PF_6$ and $7 \cdot 6PF_6$, are listed in Table 2, together with the δ values for the corresponding protons of 'free' BPP34C10 and the hexakis(hexafluorophosphate) salt $4 \cdot 6PF_6$. The ^{1}H-NMR spectrum, recorded in CD_3COCD_3 at 25 °C of BPP34C10 in its 'free' form, shows a singlet centered on δ 6.77 for the protons attached to the hydroquinone rings. For the [2]rotaxane $5 \cdot 6PF_6$, the [3]rotaxane $6 \cdot 6PF_6$, and the [4]rotaxane $7 \cdot 6PF_6$ incorporating one, two and three macrocyclic components, respectively, the hydroquinone rings protons still resonate as a singlet in each case but their signals are shifted to δ 5.96, 6.05 and 6.15, respectively. The significant changes in the chemical shifts are a consequence of the shielding effects exerted by the bipyridinium units located 'inside' the cavity of each macrocyclic polyether. In addition, the [2]rotaxane $5 \cdot 6PF_6$ and the [3]rotaxane $6 \cdot 6PF_6$ incorporate two and one 'free' bipyridinium units, respectively, which can sustain 'alongside' π–π stacking interactions with the hydroquinone rings of the macrocyclic polyether component(s) already incorporated within the rotaxanes, giving rise to more pronounced shielding effects—*i.e.*, higher $-\Delta\delta$ values. Thus, the chemical shift change associated with the resonances of the hydroquinone ring protons is inversely proportional to the number of macrocyclic components incorporated within the rotaxane assemblies. Interestingly, a linear correlation (Fig. 2) is observed between the δ values and the number of macrocyclic components $n - 1$ incorporated within such [*n*]rotaxanes.

The ^{1}H-NMR spectrum, recorded in CD_3COCD_3 at 25 °C, of the hexakis(hexafluorophosphate) salt $4 \cdot 6PF_6$ shows (Fig. 3a) only two doublets of equal intensities centered on δ 9.42 and 9.26 for the two sets of hydrogen atoms in the α-positions with respect to the nitrogen atoms in the bipyridinium units. By incorporating one macrocyclic component, the C_3 sym-

Table 1 Electrospray mass spectrometry data[a,b] for the hexakis(hexafluorophosphate) salt $4 \cdot 6PF_6$ and the rotaxanes $5 \cdot 6PF_6$, $6 \cdot 6PF_6$, and $7 \cdot 6PF_6$

Compound	M[c]	$[2M - 3PF_6]^{3+}$	$[M - 2PF_6]^{2+}$	$[M - 3PF_6]^{3+}$
$4 \cdot 6PF_6$	(3373)	2106	1543	—[e]
$5 \cdot 6PF_6$	(3909)	2464	1811	—[e]
$6 \cdot 6PF_6$	(4446)	2821	2080	1338
$7 \cdot 6PF_6$	(4982)	—[d]	2348	1517

[a] ES-MS spectra were obtained using a VG Prospec triple-focusing magnetic sector instrument operating at 4 kV accelerating voltage and fitted with an electrospray ion source. Solvent delivery to the spraying capillary employed a Jasco HPLC pump operating at a flow rate of 40 μL min^{-1}. Solutions of samples (5–10 pmol μL^{-1} in MeCN) were introduced into the solvent flow *via* a Rheodyne model 7125 injection valve with a 20 μL loop. [b] The measured masses correspond to the centroids of the unresolved isotopic distributions for each species. The peaks corresponding to the molecular ions and $[M - PF_6]^+$ species are outside the mass range scanned. [c] The molecular weights M are listed in parentheses. [d] Outside the mass range scanned. [e] Not observed.

Table 2 Chemical shifts (δ) for the hydrogen atoms in the α- and β-positions with respect to the nitrogen atoms on the bipyridinium units and for the hydrogen atoms attached to the hydroquinone rings incorporated within the macrocyclic components in CD_3COCD_3 at 25 °C

Compound	α-CH	β-CH	ArH
BPP34C10	—	—	6.77
4·6PF_6 [a]	9.42, 9,26	8.69, 8.64	—
5·6PF_6 [b]	9.37, 9.29, 9.09, 9.02	8.59, 8.54, 8.17-8.09	5.96
6·6PF_6 [b]	9.32, 9.24, 9.15, 9.12	8.52, 8.36, 8.28-8.19	6.05
7·6PF_6 [c]	9.20, 9.11	8.31, 8.27	6.15

[a] The ^{1}H-NMR spectrum shows two pairs of doublets for the α- and for the β-protons. [b] The ^{1}H-NMR spectrum shows four doublets for the α- and two doublets and one multiplet for the β-protons.

metry is lost and the ^{1}H-NMR spectrum of the [2]rotaxane **5**·6PF_6 shows (Fig. 3b) two doublets integrating each for four protons at δ 9.37 and 9.29, as well as two more doublets, each integrating for two protons at δ 9.09 and 9.02. The more intense signals observed at lower fields correspond to the α-protons on the 'free' bipyridinium units, while the α-protons on the bipyridinium unit encircled by the macrocyclic component resonate at higher fields as a result of shielding effects exerted by the sandwiching hydroquinone rings. For the [3]rotaxane **6**·6PF_6 incorporating two macrocyclic components, four doublets for the α-protons are still observed as shown in Fig. 3(c). However, now the two doublets at lower fields (δ 9.32 and 9.24) are the less intense, integrating each for two of the four α-protons of the 'free' bipyridinium recognition site, while the two partially overlapping doublets centered on δ 9.09 and 9.02 integrate for a total of eight protons—*i.e.*, the α-protons of the two 'occupied' bipyridinium recognition sites. In the case of the [4]rotaxane **7**·6PF_6, the introduction of a third macrocyclic component onto the hexacationic backbone restores the original C_3 symmetry and only two doublets of equal intensity are observed. Nonetheless, these signals resonate at higher fields (δ 9.20 and 9.11) than in the case of the hexakis(hexafluorophosphate) salt **4**·6PF_6, once again as a result of the shielding effect suffered by the protons on the bipyridinium units encircled by the macrocyclic polyether. Similar changes in the δ values and in the number of signals associated with the β-protons are observed (Table 2) in the ^{1}H-NMR spectra of **4**·6PF_6 and of the rotaxanes **5**·6PF_6, **6**·6PF_6 and **7**·6PF_6 as a result of the variation of the symmetry and of the magnitude of the shielding effect.

The hexacationic salt **4**·6PF_6 possesses a highly-charged bipyridinium-based hydrophilic core surrounded by hydrophobic tetraarylmethane-based stoppers and, as a result of its amphiphilic nature, it is perhaps not surprising that it forms aggregates[10] in low polarity solvents, such as $CHCl_3$ and CH_2Cl_2. The ^{1}H-NMR spectra of **4**·6PF_6, recorded in either CD_3CN or CD_3COCD_3 (Fig. 4a and 4b, respectively) at room temperature, show sharp and well-resolved resonances. On the contrary, when the relatively low polarity solvent $CDCl_3$ is employed (Fig. 4c), broad resonances are observed over a wide range of concentrations (10^{-2}–10^{-3} M) and temperatures (−60 to +30 °C). These results suggest that, as a result of the relatively low degree of solvation achieved in

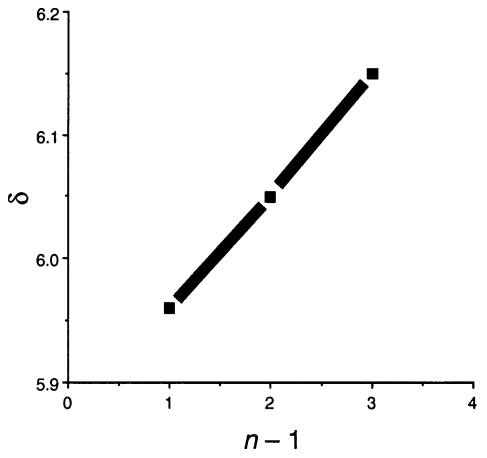

Fig. 2 Plot of the chemical shifts δ for the hydrogen atoms attached to the hydroquinone rings of the macrocyclic polyether components *versus* the number of macrocyclic components ($n-1$) incorporated within the [n]rotaxanes **5**·6PF_6, **6**·6PF_6 and **7**·6PF_6

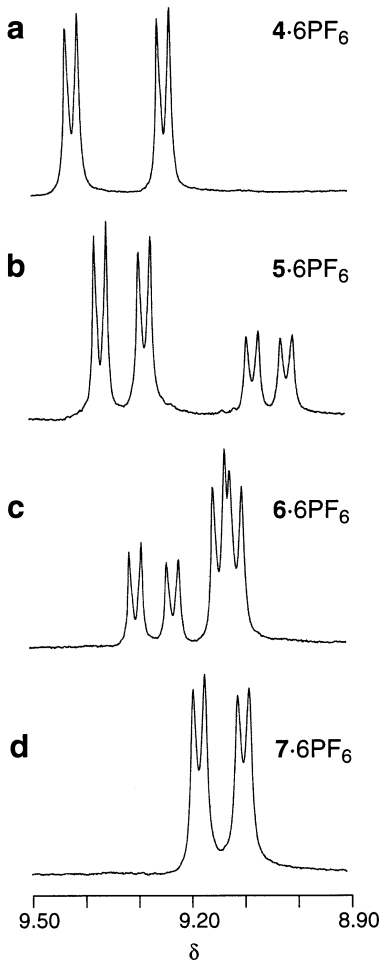

Fig. 3 Partial ^{1}H-NMR spectra of (a) the hexakis(hexafluorophosphate) salt **4**·6PF_6 and the [n]rotaxanes (b) **5**·6PF_6, (c) **6**·6PF_6 and (d) **7**·6PF_6 in CD_3COCD_3 at room temperature, showing the resonances for the hydrogen atoms in the α-positions with respect to the nitrogen atoms on the bipyridinium units

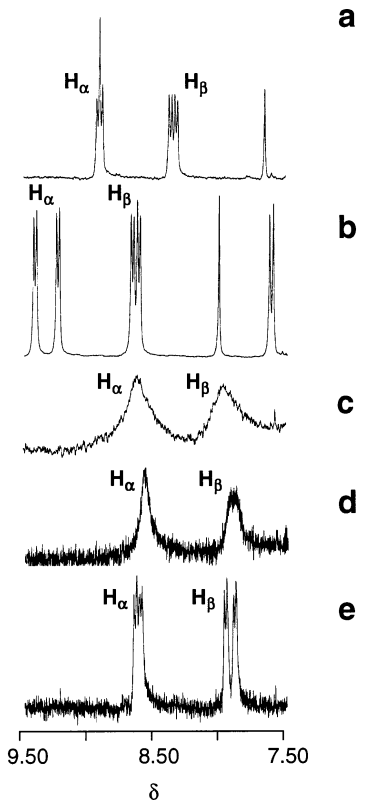

Fig. 4 Partial ^{1}H-NMR spectra of the hexakis(hexafluorophosphate) salt $\mathbf{4}\cdot 6PF_6$ in (a) CD_3CN, (b) CD_3COCD_3, (c) $CDCl_3$, (d) $CDCl_3$–CD_3COCD_3 (85 : 15), and (e) $CDCl_3$–CD_3COCD_3 (70 : 30) at room temperature, showing the resonances for the hydrogen atoms in the α-positions (H_α) and the β-positions (H_β) with respect to the nitrogen atoms on the bipyridinium units

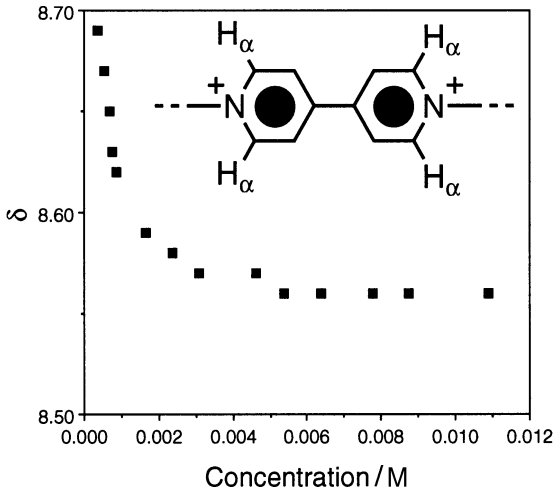

Fig. 5 Plot of the chemical shifts (δ) corresponding to the center of the multiplet associated with the hydrogen atoms H_α in the α-positions with respect to the nitrogen atoms on the bipyridinium units of $\mathbf{4}\cdot 6PF_6$ against the molar concentration in $CDCl_3$–CD_3COCD_3 (70 : 30) at room temperature

$CDCl_3$, the hexacationic cores of independent molecules of $\mathbf{4}\cdot 6PF_6$ and their counter ions form aggregates in solution. Titration of a $CDCl_3$ solution of $\mathbf{4}\cdot 6PF_6$ (10^{-3} M) with CD_3COCD_3 results in gradual sharpening (Fig. 4d) of the resonances in the ^{1}H-NMR spectra. After the addition of *ca.* 30% of CD_3COCD_3, the aggregates are dismembered and sharp resonances are observed as shown in Fig. 4e. The concentration dependence of the chemical shift δ of the hydrogen atoms H_α in the α-positions with respect to the nitrogen atoms on the bipyridinium units in $CDCl_3$–CD_3COCD_3 (70 : 30) at room temperature is illustrated in Fig. 5. Significant changes in the δ values are observed at low concentrations ($<10^{-3}$ M), as a result of the equilibration of $\mathbf{4}\cdot 6PF_6$ in its 'free' and aggregate forms. On the contrary, full aggregation is achieved at higher concentrations ($>10^{-3}$ M) and no relevant changes in the δ values are observed. Optical microscopic investigation of $CHCl_3$ solutions of $\mathbf{4}\cdot 6PF_6$ of various concentrations (10^{-2}–10^{-4} M) did not reveal any lyotropic state. Nonetheless, the formation of a gel was observed after the slow liquid–liquid diffusion of hexane into a $CHCl_3$ solution of $\mathbf{4}\cdot 6PF_6$ (10^{-3} M). Examination of the gel formed after slow evaporation of the solvent from a THF solution of $\mathbf{4}\cdot 6PF_6$ by field-emission scanning electron microscopy (FE-SEM) revealed (Fig. 6) the formation of regular plate-like fragments with a size of approximately 100–200 nm.

Absorption and luminescence properties

The compounds examined in this paper are particularly interesting species from the viewpoint of absorption and luminescence properties since they contain a number of chromophoric units. Some of these units are relatively isolated, whereas others interact more or less strongly. In this regard, a comparison between the properties of suitable model compounds for each chromophoric unit and the properties of the triply-branched compound $\mathbf{4}^{6+}$ and its [*n*]rotaxanes $\mathbf{5}^{6+}$, $\mathbf{6}^{6+}$, and $\mathbf{7}^{6+}$ can be enlightening.

The chromophoric units that can be singled out in the examined compounds are of the following types (Fig. 7): methoxybenzene (MB), *p*-dimethoxybenzene (PDMB), *p*-methoxytriphenylmethane derivative stopper (S), and dibenzylbipyridinium dication (DBV). For example, the [2]rotaxane $\mathbf{5}^{6+}$ is composed of a BPP34C10 macrocycle, which contains two PDMB-type chromophoric groups, and the $\mathbf{4}^{6+}$ component, which contains three DBV-type, three MB-type and three S-type units.

The most relevant absorption and emission data are collected in Table 3. The absorption and emission spectra (MeCN solution, room temperature) of the model compounds[5f,g,11,12] MB, PDMB, DBV and S are shown in Fig. 8*a*. The absorption spectrum of the branched compound $\mathbf{4}^{6+}$ is compared with the sum of the spectra of its component units in Fig. 8*b*, and the spectra of the branched rotaxanes $\mathbf{5}^{6+}$, $\mathbf{6}^{6+}$, and $\mathbf{7}^{6+}$ are displayed in Fig. 9. None of the component units shows absorption bands above 310 nm. MB, PDMB and S exhibit a strong fluorescence band in the 280–

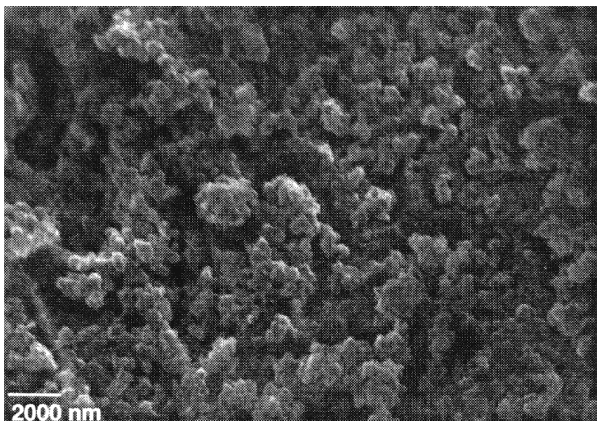

Fig. 6 Field-emission scanning electron micrograph of the gel formed by slow evaporation of the solvent from a THF solution of $\mathbf{4}\cdot 6PF_6$

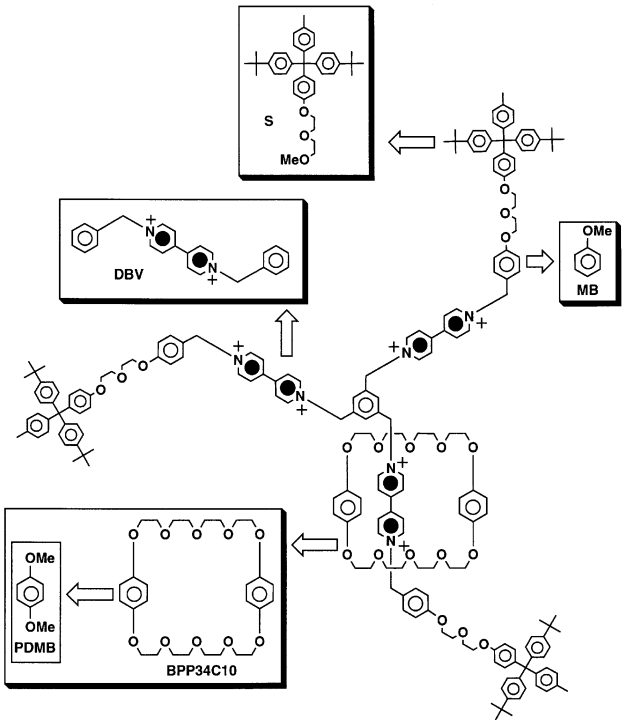

Fig. 7 Chromophoric and electroactive units that can be identified in the [2]rotaxane $\mathbf{5}^{6+}$

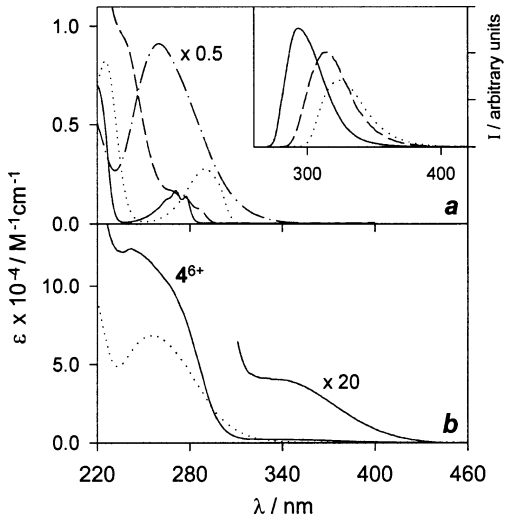

Fig. 8 (*a*) Absorption spectra (MeCN solution, room temperature) of the model compounds MB (———), PDMB (·····), DBV (–·–·–), and S (– – – –); the inset shows the emission spectra of MB (———), PDMB (·····), and S (– – – –) under the same conditions. (*b*) Absorption spectrum of the branched compound $\mathbf{4}^{6+}$ (———) compared with the sum of the spectra of its component units (·····)

360 nm spectral range, whereas DBV does not show any luminescence. As previously observed,[5f,11] the absorption spectrum of the BPP34C10 macrocycle has the shape expected for two PDMB units, but it is less intense; its fluorescence spectrum is identical to that of PDMB, except for a lower (*ca.* 30%) intensity.

The triply-branched compound $\mathbf{4}^{6+}$ contains both electron-acceptor (DBV) and electron-donor (MB and S) units, as does the previously investigated thread-type compound formally derived from $\mathbf{4}^{6+}$ by cutting one of its three arms.[5f] One could therefore expect the presence of intramolecular charge-transfer (*intra*-CT) bands, as is indeed the case [Fig. 8*b*]. The broad and weak band in the near-UV region ($\lambda_{max} \approx 340$ nm), which is present also in the bis(*p*-methoxydibenzyl)bipyridinium dication,[5f] can be assigned to the interaction between the directly connected methoxybenzene and bipyridinium units. From the absorption spectra, nothing can be said about the interaction of the stoppers with the bipyridinium units. The presence of an *intra*-CT excited state below the luminescent excited states of the MB-type units of $\mathbf{4}^{6+}$ has important consequences on the emission properties, since such a CT state introduces a fast radiationless deactivation route, thereby

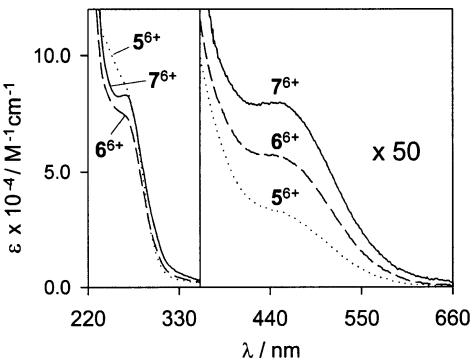

Fig. 9 Absorption spectra of the branched rotaxanes $\mathbf{5}^{6+}$ (·····), $\mathbf{6}^{6+}$ (– – – –), and $\mathbf{7}^{6+}$ (———)

Table 3 Absorption, luminescence, and electrochemical properties

	Absorption[a]		Luminescence[a]			Electrochemistry[b]	
Compound	λ_{max}/nm	ε/M^{-1} cm^{-1}	λ_{max}/nm	Φ	τ/ns	$E^{red}_{1/2}$/V *vs.* SCE	E^{ox}/V *vs.* SCE[c]
MB[d]	277	1400	293	0.10	5.0	—	+1.8
PDMB[d]	290	2800	320	0.11	2.5	—	+1.3
BPP34C10	290[d]	5200[d]	320[d]	0.08[d]	2.5[d]	—	+1.28;[e] +1.37[e]
S[d]	270	2600	314	0.08	4.5	—	+1.5
DBV[f]	259	18000	—	—	—	-0.35; -0.78	—
$\mathbf{4}^{6+}$	240	12500	313	$\leqslant 5 \times 10^{-4}$	$<0.5^{g}$	-0.32 (3); -0.77[h]	$\approx +1.5$[i]
	340	2000					
$\mathbf{5}^{6+}$	250	9000	—	—	—	-0.33 (2);[j] -0.43;[j]	+1.4; +1.5[i]
	440	800				-0.76 (2); -0.83[h]	
$\mathbf{6}^{6+}$	250	7500	—	—	—	-0.31;[j] -0.43 (2);[j]	+1.4; +1.5[i]
	440	1200				-0.76 (2);[j] -0.86 (2)[j]	
$\mathbf{7}^{6+}$	250	8000	—	—	—	-0.42 (3); -0.85 (3)	+1.4; +1.6[i]
	440	1600					

[a] MeCN solution, 298 K. [b] Argon-purged MeCN solution, 298 K; halfwave potential values in V *vs.* SCE; reversible and monoelectronic processes, unless otherwise noted; for reversible processes, the number of exchanged electrons is indicated in parentheses. [c] All oxidation processes are not fully reversible; potential values estimated from DPV peaks. [d] Data from ref. 5(*f*). [e] Data from ref. 11. [f] Data from ref. 12. [g] A long-lived component ($\tau \approx 5$ ns) is assigned to the presence of an S-type impurity. [h] Affected by adsorption phenomena. [i] Other irreversible waves follow up to 2.0 V. [j] Potential values estimated from the DPV scan after deconvolution fit of the peak profiles.[13]

quenching the MB-type fluorescence (Table 3). Interestingly, in $\mathbf{4}^{6+}$ there is some weak, residual fluorescence at 313 nm, indicating that the strong fluorescence of the S units is substantially, but not completely, quenched.

The absorption spectra of the branched rotaxanes $\mathbf{5}^{6+}$, $\mathbf{6}^{6+}$, and $\mathbf{7}^{6+}$ are shown in Fig. 9. In the spectrum of the [2]rotaxane $\mathbf{5}^{6+}$, the *intra*-CT band around 340 nm of the $\mathbf{4}^{6+}$ component can no longer be seen because it is covered by a high intensity tail, and another broad absorption band is present around 450 nm. Such a band, which is typical of rotaxanes made of a bipyridinium-type unit surrounded by a BPP34C10 macrocycle,[5f] can be assigned to a charge-transfer transition involving the electron-donor PDMB-type units of the BPP34C10 macrocycle and the electron-acceptor DBV-type unit of the $\mathbf{4}^{6+}$ component. Such a band and the corresponding electronic transition are indicated by *inter*-CT to avoid confusion with the above discussed *intra*-CT found in the 'free' triply-branched compound $\mathbf{4}^{6+}$.

As far as luminescence is concerned, the spectrum of the [2]rotaxane $\mathbf{5}^{6+}$ differs strongly from the sum of the spectra of its two separated components BPP34C10 and $\mathbf{4}^{6+}$ (Table 3). Neither the weak emission band of the S-type unit of $\mathbf{4}^{6+}$, nor the strong emission band of the BPP34C10 macrocycle are present. This result can be accounted for by the charge-transfer interaction, already evidenced by the absorption spectra, between the macrocycle and the bipyridinium unit of $\mathbf{4}^{6+}$. The *inter*-CT excited state, in fact, lies below the fluorescent excited state of S and BPP34C10, and therefore offers a fast radiationless deactivation route to such levels.

The [3]rotaxane $\mathbf{6}^{6+}$ and the [4]rotaxane $\mathbf{7}^{6+}$ differ from the [2]rotaxane $\mathbf{5}^{6+}$ because of the additional presence of a second and, respectively, a third BPP34C10 macrocycle. It is therefore expected that the *inter*-CT absorption band becomes twice and, respectively, three times more intense than that of $\mathbf{5}^{6+}$. Although an increase in the absorption intensity is clearly observed (Fig. 9), quantitatively the increase is lower than expected. This result can be accounted for by two different effects: (*i*) in the [2]rotaxane, and, to a lesser extent in the [3]rotaxane, the bipyridinium units not encircled by a crown ether can be engaged in 'alongside' donor–acceptor interactions with the crown ether encircling another bipyridinium unit, thereby increasing the intensity of the CT band; (*ii*) steric crowding could preclude optimization of the donor–acceptor interactions in the [3]- and [4]-rotaxanes, which would imply a small contribution to the CT band. The first effect is supported by a comparison with the CT absorption band of a [2]rotaxane composed of BPP34C10 and a simple thread corresponding to one arm of $\mathbf{4}^{6+}$. In such a compound, the *inter*-CT absorption band is about 40% less intense than that of $\mathbf{5}^{6+}$. No emission can be observed for $\mathbf{6}^{6+}$ and $\mathbf{7}^{6+}$ for the same reason as discussed in the case of $\mathbf{5}^{6+}$.

Electrochemical properties

As with the spectroscopic properties, it is convenient to discuss the electrochemical properties of the branched compound $\mathbf{4}^{6+}$ and its [*n*]rotaxanes by comparison with the properties of model compounds of their electroactive units. Such model compounds are again the previously studied[5f,g,11,12] methoxybenzene (MB), *p*-dimethoxybenzene (PDMB), *p*-methoxytriphenyl-methane derivative stopper (S), and dibenzylbipyridinium dication (DBV) (Fig. 7). The electrochemical properties of the branched compound $\mathbf{4}^{6+}$ and the branched rotaxanes $\mathbf{5}^{6+}$, $\mathbf{6}^{6+}$, and $\mathbf{7}^{6+}$ are displayed in Table 3, where the electrochemical properties of the BPP34C10 crown ether and of the model compounds[5f,g,11] are also shown for comparison purposes. In general, the reduction processes, which involve the bipyridinium-like units, are reversible, whereas the oxidation processes are not fully reversible.

The triply-branched compound $\mathbf{4}^{6+}$ shows a reversible three-electron reduction wave at -0.32 V and a following wave at *ca.* -0.77 V strongly disturbed by electrode adsorption. A thread-type compound formally derived from $\mathbf{4}^{6+}$ by cutting one of its three arms was previously shown to exhibit two reversible bielectronic processes at -0.33 and -0.78 V, assigned to the simultaneous first and, respectively, second reduction of its two bipyridinium units.[5f] By comparison, the two processes observed for $\mathbf{4}^{6+}$ can therefore be assigned to the simultaneous first and, respectively, second reductions of its three bipyridinium units.

On oxidation, the electroactive units of $\mathbf{4}^{6+}$ are expected to be the three MB- and three S-type units. We have found several irreversible waves in a very positive range of potential (the first wave is at *ca.* $+1.5$ V), where the oxidation of the MB and S model compounds take place[5f] (Table 3). Specific assignments, however, are precluded by the irreversible nature of the observed processes.

The branched rotaxanes $\mathbf{5}^{6+}$, $\mathbf{6}^{6+}$, and $\mathbf{7}^{6+}$, besides the electroactive units of the triply-branched backbone $\mathbf{4}^{6+}$, contain the BPP34C10 macrocycle whose two PDMB-type units are oxidized at distinct potentials:[11] the first oxidation wave practically coincides with that of PDMB, whereas the second one is displaced to a slightly more positive potential. In the [2]rotaxane $\mathbf{5}^{6+}$, one of the three bipyridinium-type units is engaged in electron-donor–acceptor interactions with the crown ether, and is therefore expected to be reduced at a more negative potential than the other ones. In accordance with these expectations, we have found four waves: (*i*) a bielectronic wave at -0.33 V (*i.e.*, at a potential very close to that found for the first reduction of $\mathbf{4}^{6+}$),[14] assigned to the simultaneous reduction of the two 'free' bipyridinium-type units; (*ii*) a monoelectronic wave at more negative potential (-0.43 V), assigned to the first reduction of the bipyridinium-type unit encircled by the crown ether; (*iii*) a bielectronic wave at -0.76 V, assigned to the simultaneous second reduction of the two 'free' bipyridinium-type units; (*iv*) a fourth wave around -0.83 V, perturbed by adsorption phenomena, which can be assigned to the second reduction of the bipyridinium-type unit encircled by the crown ether. The same reduction pattern, except for the number of exchanged electrons, was observed for the [2]rotaxane made of a BPP34C10 macrocycle and the previously mentioned thread-type compound containing only two electroactive bipyridinium-type units.[5f] On oxidation, the [2]rotaxane $\mathbf{5}^{6+}$ shows a wave, not present in $\mathbf{4}^{6+}$, at $+1.4$ V, which can be assigned to oxidation of the crown ether. Because of the charge-transfer interaction, oxidation occurs at a more positive potential than the first oxidation wave of the free crown ether.[5f,11] Furthermore, even if the process is not fully reversible, it seems that oxidation of the two PDMB-type units of the crown ether occurs at the same potential, contrary to what is observed for the free crown ether (Table 3). This different behaviour is most likely due to the fact that the two PDMB-type units of the crown ether in the [2]rotaxane are prevented from interacting by the interposed bipyridinium-type unit. At more positive potentials ($\geqslant +1.5$ V), irreversible oxidation waves are present, on account of the S- and MB-type units of the $\mathbf{4}^{6+}$ component.

The electrochemical behaviour of [3]rotaxane $\mathbf{6}^{6+}$ can be straightforwardly explained on the basis of the above discussion. On reduction, a first monoelectronic wave, assigned to the first reduction of the 'free' bipyridinium-type unit, is followed by a bielectronic wave, assigned to the first reduction of the two bipyridinium-type units encircled by the crown ether. Even the second reduction of the three bipyridinium-type units, which occurs at more negative potentials, takes place with the same 1 : 2 pattern. On oxidation, the behaviour of [3]rotaxane $\mathbf{6}^{6+}$ is again similar to that of [2]rotaxane $\mathbf{5}^{6+}$, with a more intense wave in correspondence of oxidation of the PDMB-type units. In the [4]rotaxane $\mathbf{7}^{6+}$, the three

bipyridinium-type units are expected to be electrochemically equivalent since each one is encircled by a crown ether. In agreement with this expectation, we have found two tri-electronic waves corresponding to the first and second reduction of the bipyridinium-type units, a situation similar to that observed for the $\mathbf{4}^{6+}$ backbone. In the case of the [4]rotaxane, the waves occur at more negative potentials because of the CT interaction. As far as oxidation is concerned, the behaviour of $\mathbf{7}^{6+}$ is in line with that of $\mathbf{6}^{6+}$ and $\mathbf{5}^{6+}$.

The correlation of the electrochemical properties of $\mathbf{4}^{6+}$ and its [2]-, [3]-, and [4]-rotaxanes is nicely illustrated by Fig. 10, where the DPV peaks corresponding to the first reduction of the bipyridinium-type units are shown. In going from $\mathbf{4}^{6+}$ to $\mathbf{7}^{6+}$, the areas of the peak at -0.32 V decrease with a decreasing number of free bipyridinium-type units and, in parallel, the areas of the peak at -0.42 V increase with an increasing number of encircled bipyridinium-type units. It should also be noted that the DPV peak of $\mathbf{7}^{6+}$ is broader than that of $\mathbf{4}^{6+}$, presumably because in $\mathbf{7}^{6+}$ the single [2]rotaxane subunits may have slightly different equilibrium conformations because of steric constraints, in agreement with the observation made above on the relative intensity of the *inter*-CT band of the [*n*]rotaxanes. Correlations for the other electrochemical processes are made difficult by the lack of full reversibility and/or presence of electrode adsorption phenomena.

Molecular modeling

In order to visualize the tridimensional structures of the rotaxanes $\mathbf{5}^{6+}$, $\mathbf{6}^{6+}$, and $\mathbf{7}^{6+}$ and to explain the formation of aggregates for the triply-branched backbone $\mathbf{4}^{6+}$ in low polarity solvents, a molecular modeling investigation was performed. In particular, the rotaxanes were subjected individually to simulated annealing employing the AMBER* force field and the GB/SA solvation model for H_2O as implemented in Macromodel 5.0.[15] A space-filling representation of the global minimum found for the [4]rotaxane $\mathbf{7}^{6+}$ is shown in Fig. 11.

For the triply-branched backbone $\mathbf{4}^{6+}$, a dimeric aggregate incorporating twelve acetate[16] counter ions was constructed manually in the input mode of Macromodel 5.0. The dimer was subjected to simulated annealing employing the AMBER* force field and the GB/SA solvation model for $CHCl_3$. In the resulting global minimum, the polycationic core of the two individual monomers and their associated counter ions are stacked (Fig. 12) to afford a highly localized polar central region, while the polyether chains and appended tetraarylmethane groups extend into the bulk solvent. On the contrary, when the simulated annealing was repeated employing the GB/SA solvation model for H_2O, a global minimum

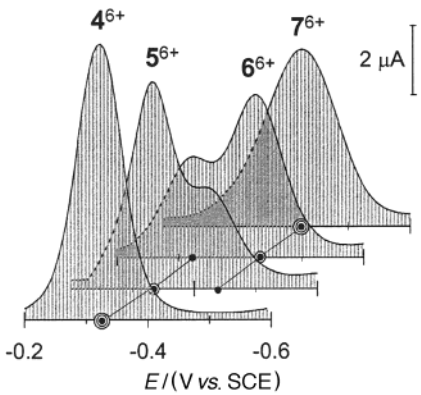

Fig. 10 DPV peaks corresponding to the first reduction of $\mathbf{4}^{6+}$ and its [2]-, [3]-, and [4]-rotaxanes. The circles indicate the number of electrons exchanged. The current intensity has been corrected to take into account differences in diffusion coefficients

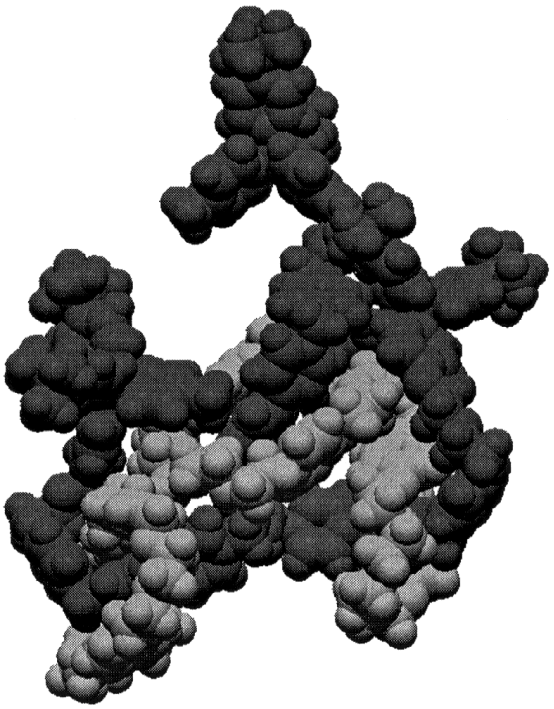

Fig. 11 Space-filling representation of the global minimum found for the [4]rotaxane $\mathbf{7}^{6+}$ after simulated annealing

with the two triply-branched molecules well separated from each other was obtained.

Langmuir films[17]

Despite the absence of long alkyl chains, the triply-branched compound $\mathbf{4}\cdot 6PF_6$ and the rotaxanes $\mathbf{5}\cdot 6PF_6$, $\mathbf{6}\cdot 6PF_6$ and $\mathbf{7}\cdot 6PF_6$ form stable Langmuir monolayer films at the air–water interface. The surface-pressure–area (π–A) isotherms of the monolayers revealed (Fig. 13) two steps in all cases—*i.e.*, each of the four compounds generates two different types of aggregate. Presumably, the transition from the first to the second aggregate is a result of conformational changes which lead from 'expanded' to relatively 'compact' and more densely packed molecules. For $\mathbf{4}\cdot 6PF_6$, a value of the limiting area per molecule of 580 Å^2 was measured (Table 4) for the first step. By increasing the pressure, a second step was observed corresponding to a more densely packed monolayer with an associated limiting area per molecule of 370 Å^2. For

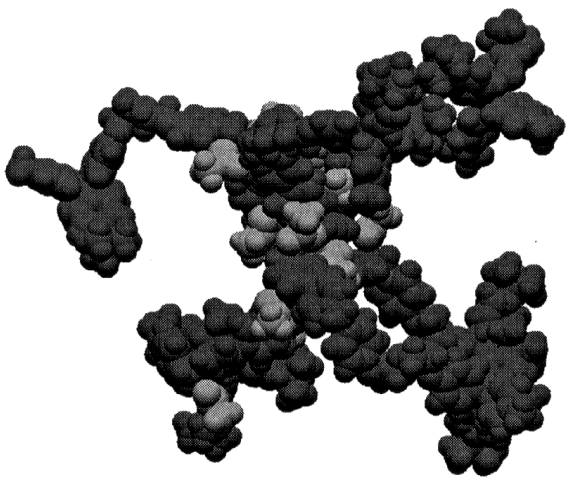

Fig. 12 Space-filling representation of the global minimum found for a dimeric aggregate of $4\cdot 6AcO$ after simulated annealing performed employing the GB/SA solvation model for $CHCl_3$

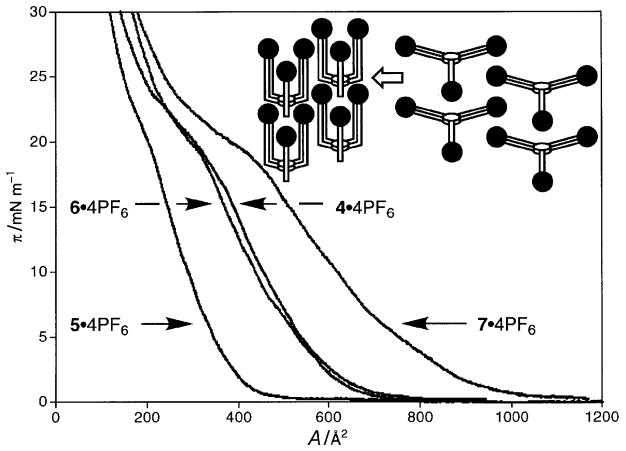

Fig. 13 Surface-pressure–area (π–A) isotherms measured for the 'free' backbone $\mathbf{4}\cdot 6PF_6$ and for the rotaxanes $\mathbf{5}\cdot 6PF_6$, $\mathbf{6}\cdot 6PF_6$ and $\mathbf{7}\cdot 6PF_6$

the rotaxanes, the values of the limiting area per molecule associated with the first step (370, 550 and 810 Å^2 for $\mathbf{5}\cdot 6PF_6$, $\mathbf{6}\cdot 6PF_6$ and $\mathbf{7}\cdot 6PF_6$, respectively) and those associated with the second step (230, 370 and 410 Å^2 for $\mathbf{5}\cdot 6PF_6$, $\mathbf{6}\cdot 6PF_6$ and $\mathbf{7}\cdot 6PF_6$, respectively) increase with the number of macrocyclic components incorporated within the rotaxane. A similar trend is observed (Table 4) for the differences between the values of the limiting area per molecule associated with the first step and those associated with the second which, again, increase with the number of macrocyclic components incorporated within the rotaxane. These results suggest that the higher the number of macrocyclic components (*i*) the more 'expanded' the geometries of the individual rotaxane molecules are within the monolayers, as a result of steric congestion, and (*ii*) the more significant the differences between the geometries adopted by each rotaxane in the first and second step are. In addition, presumably as a result of intermolecular π–π stacking interactions involving the two 'free' bipyridinium recognition sites and the 'outer faces' of the two hydroquinone rings incorporated within the macrocyclic component, the two distinct monolayers formed by the [2]rotaxane $\mathbf{5}\cdot 6PF_6$ are more densely packed than those associated with the less bulky 'free' backbone compound $\mathbf{4}\cdot 6PF_6$ which behaves instead in a manner that is extremely reminiscent of the [3]rotaxane $\mathbf{6}\cdot 6PF_6$.

Table 4 Values of the limiting area per molecule measured for the Langmuir films associated with the hexakis(hexafluorophosphate) salt $\mathbf{4}\cdot 6PF_6$ and the rotaxanes $\mathbf{5}\cdot 6PF_6$, $\mathbf{6}\cdot 6PF_6$ and $\mathbf{7}\cdot 6PF_6$ at air–water interface

Compound	A_1[a]/Å^2	A_2[b]/Å^2	ΔA[c]/Å^2
$\mathbf{4}\cdot 6PF_6$	580	370	210
$\mathbf{5}\cdot 6PF_6$	370	230	140
$\mathbf{6}\cdot 6PF_6$	550	370	180
$\mathbf{7}\cdot 6PF_6$	810	410	400

[a] Limiting area per molecule associated with the first step observed (Fig. 13) in the surface-pressure–area (π–A) isotherms. [b] Limiting area per molecule associated with the second step observed in the π–A isotherms. [c] Difference between the values of the limiting area per molecule measured for the first and second steps of the π–A isotherms ($\Delta A = A_1 - A_2$).

Atomic force microscopy

The two distinct monolayers associated with each of the compounds $\mathbf{4}\cdot 6PF_6$, $\mathbf{5}\cdot 6PF_6$, $\mathbf{6}\cdot 6PF_6$ and $\mathbf{7}\cdot 6PF_6$ at the air–water interface were transferred onto freshly cleaved mica while the surface pressure was maintained at 15 and 30 mN m^{-1} and then analyzed by atomic force microscopy (AFM). In the 'free' backbone compound $\mathbf{4}\cdot 6PF_6$, the AFM micrographs showed (Fig. 14) a marked difference in the shape of its two monolayers. The first monolayer (limiting area per molecule 580 Å^2) in the surface-pressure–area (π–A) isotherm possesses well-defined domains—*i.e.*, 'hills'—with diameters of *ca.* 55.6 nm, as revealed (Table 5) by its section analysis. On the contrary, in the second monolayer (limiting area per molecule 370 Å^2) in the π–A isotherm, the diameter of the 'hills' shrinks to *ca.* 15.8 nm. In the [2]rotaxane $\mathbf{5}\cdot 6PF_6$, where the difference in the values of the limiting area per molecule of the first and second steps in the π–A isotherm is only 140 Å^2, the changes in the shapes of its first and second monolayers are (Fig. 15) less evident. Again, the section analysis revealed an irregular profile with the diameter of the 'hills' and the

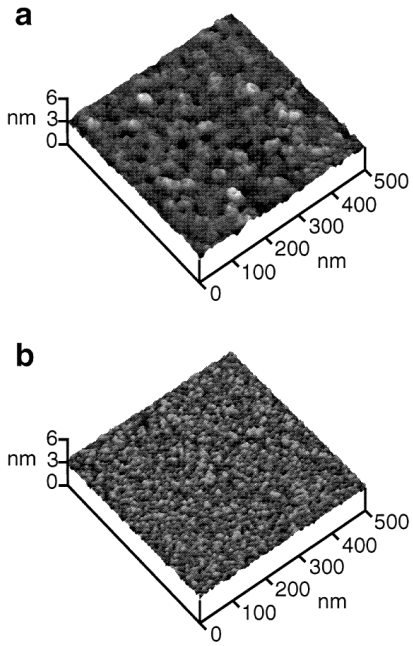

Fig. 14 Atomic force micrographs of the (a) first and (b) second monolayers (area per molecule 580 and 370 Å^2, respectively) formed by the 'free' backbone $\mathbf{4}\cdot 6PF_6$

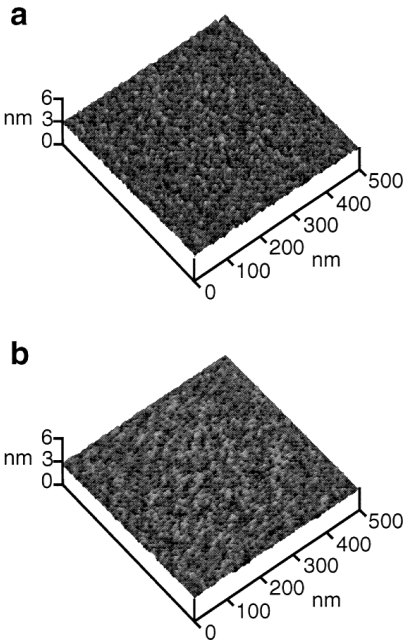

Fig. 15 Atomic force micrographs of the (a) first and (b) second monolayers (area per molecule 370 and 230 Å^2, respectively) formed by the [2]rotaxane $\mathbf{5}\cdot 6PF_6$

Table 5 Values of the heights and diameters of the 'hills' and 'valleys' associated with the section profile of the first and second monolayers of the hexakis(hexafluorophosphate) salt **4** · $6PF_6$ and of the rotaxanes **5** · $6PF_6$, **6** · $6PF_6$ and **7** · $6PF_6$

Compound		A^a/Å^2	Hills		Valleys	
			$h_1{}^b$/nm	$d_1{}^b$/nm	$h_2{}^b$/nm	$d_2{}^b$/nm
4 · $6PF_6$	Monolayer I	580	4.31	55.6		
	Monolayer II	370	4.32	15.8		
5 · $6PF_6$	Monolayer I	370	3.70	15.6	2.65	12.7
	Monolayer II	230	1.56	9.6	3.06	6.72
6 · $6PF_6$	Monolayer I[c]	550			2.22	21.1
					1.18	11.9
	Monolayer II	370			2.98	13.7
7 · $6PF_6$	Monolayer I	810	3.04	23.4		
	Monolayer II[d]	410	4.35	8.3		

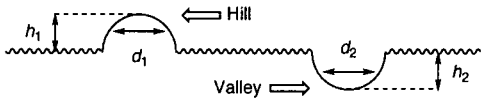

[a] Limiting area per molecule associated with the first and second monolayers of each compound, as determined (Fig. 13) from the surface-pressure–area (π–A) isotherms. [b] The heights h_1 and h_2 and the half-height diameters d_1 and d_2 are illustrated schematically in the diagram and were determined by the section analyses of the atomic force micrographs. [c] In the first monolayer on the π–A isotherm of the [3]rotaxane **6** · $6PF_6$, two different types of 'valleys' are observed. [d] The diameter of the 'craters' of the 'volcanoes' characterizing this monolayer is approximately 22.4 nm.

'valleys' decreasing from *ca.* 15.6 and 12.7 to *ca.* 9.6 and 6.7, respectively, on going from the first (limiting area per molecule 370 Å^2) to the second (limiting area per molecule 230 Å^2) monolayer. In the [3]rotaxane **6** · $6PF_6$, the difference between the shapes of the first (limiting area per molecule 550 Å^2) and second (limiting area per molecule 370 Å^2) monolayers are (Fig. 16) again very pronounced. The section analysis of the first monolayer revealed two types of 'valleys' having diameters of *ca.* 21.2 and 11.9 nm. On the contrary, the section analysis of the second monolayer showed only one type of 'valley' with a diameter of *ca.* 13.7 nm. A much more significant difference was observed (Fig. 17) between the shapes of the first and second monolayers of the [4]rotaxane **7** · $6PF_6$ where the difference in the values of the limiting area per molecule associated with its two monolayers is as high as 400 Å^2. Indeed, while the first monolayer (limiting area per molecule 810 Å^2) shows only 'hills' with a diameter of *ca.* 23.4 nm the second one (limiting area per molecule 410 Å^2) possesses 'volcanoes' with 'craters' having a diameter of *ca.* 22.4 nm and walls *ca.* 8.3 nm thick. Thus, the second monolayer includes morphologically well-defined nanometre-sized aggregates formed by the self-organization of self-assembled [4]rotaxanes.

Conclusions

Three novel [*n*]rotaxanes, incorporating a triply-branched bipyridinium-based backbone encircled by one, two, or three hydroquinone-based macrocyclic polyether components, have been self-assembled in good yields using the so-called slippage procedure. The methodology relies on (*i*) the size complementarity between the macrocyclic components and the bulky

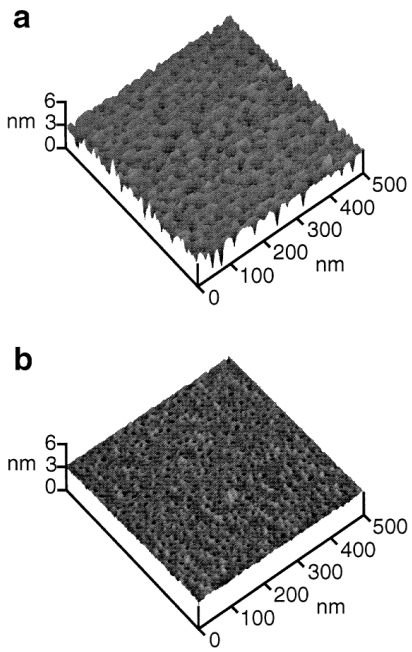

Fig. 16 Atomic force micrographs of the (a) first and (b) second monolayers (area per molecule 550 and 370 Å^2, respectively) formed by the [3]rotaxane **6** · $6PF_6$

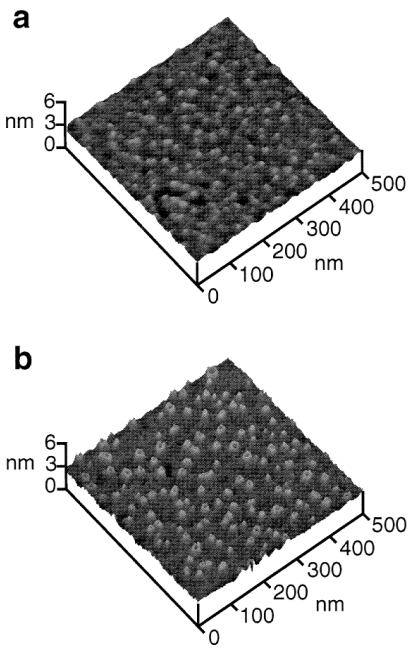

Fig. 17 Atomic force micrographs of the (a) first and (b) second monolayers (area per molecule 810 and 410 Å^2, respectively) formed by the [3]rotaxane **7** · $6PF_6$

tetraarylmethane-based stoppers attached at the periphery of the π-electron deficient backbone, as well as on (*ii*) cooperative noncovalent bonding interactions, such as π–π stacking between the complementary aromatic units and hydrogen bonding between the polyether oxygen atoms and the acidic bipyridinium hydrogen atoms. The characterization of these molecular compounds was achieved by employing spectroscopic and electrochemical techniques. The triply-branched backbone compound $\mathbf{4}^{6+}$ and its [2]-, [3]-, and [4]-rotaxanes are composed of several chromophoric and electroactive units and therefore show very interesting spectroscopic and electrochemical properties. Charge-transfer and energy-transfer processes involving different units have been investigated by absorption and luminescence experiments. Correlations among the redox potentials of the various compounds have allowed the assignment of the reduction and oxidation processes to specific electroactive units. An ^{1}H-NMR spectroscopic investigation of the hexacationic triply-branched backbone in its 'free' form revealed the formation of aggregates in solution when low polarity solvents, such as $CHCl_3$ or CH_2Cl_2, are employed. These results are consistent with molecular modeling studies showing the formation of aggregates in $CHCl_3$—but not in H_2O. In addition, the formation of a gel occurs after the slow liquid–liquid diffusion of hexane into a $CHCl_3$ solution of the triply-branched hexacationic salt. Field-emission scanning electron microscopic investigation of the gel revealed the presence of regular sized domains. Stable Langmuir monolayer films of the triply-branched hexacationic salt and of the rotaxanes were generated at the air–water interface. The surface-pressure–area isotherms revealed two steps corresponding to the formation of two distinct monolayers in each case. Consistently, atomic force microscopic analyses of the two distinct monolayers formed by each compound performed after transferring the monolayers onto mica surfaces revealed significant differences in their shapes. Furthermore, the values of the limiting area per molecule measured for the rotaxanes in both steps of the π–A isotherms increase with the number of macrocyclic components incorporated within the rotaxanes, presumably as a result of steric congestion.

The multicomponent self-assembly of the branched [*n*]rotaxanes in good yields demonstrates the potential of slippage to generate precisely and efficiently wholly-synthetic interlocked molecular compounds. The relative simplicity of this procedure suggests the possibility of constructing more complex macromolecular systems such as main-, side-chain, and dendritic oligo- and poly-rotaxanes. Furthermore, not only the forms but also the functions of the resulting molecular structures and supramolecular superstructures can be engineered and controlled by introducing electrochemically- and/or photochemically-active subunits in order to generate functioning nanometre-sized molecular and supramolecular device-like systems.[18]

Experimental

General methods

Chemicals were purchased from Aldrich and used as received. Solvents were dried [MeCN (from P_2O_5), DMF (from CaH_2)] according to literature procedures.[19] The macrocyclic polyether BPP34C10,[11] the tribromide **1**,[20] and the tetraarylmethane-based chloride **3**[5f] were prepared according to published procedures. Reactions requiring ultra-high pressures were carried out in Teflon vessels using a custom-built ultra-high pressure reactor manufactured by PSIKA Pressure Systems Limited of Glossop, UK. Thin layer chromatography (TLC) was carried out on aluminium sheets coated with silica-gel 60 (Merck 5554), and column chromatography on silica-gel 60 (Merck 9385, 230-400 mesh). Melting points were determined on an Electrothermal 9200 melting point apparatus and are uncorrected. Microanalyses (in %) were performed by the University of Birmingham Microanalytical Services. Liquid secondary ion mass spectrometry (LSI-MS), in conjunction with a 3-nitrobenzyl alcohol or 2-nitrophenyloctyl ether matrix, was performed on a VG Zabspec instrument. Electrospray mass spectra (ES-MS) were measured on a VG Prospec mass spectrometer. ^{1}H-NMR Spectra were recorded on a Bruker AC300 (300 MHz) spectrometer, and ^{13}C-NMR spectra on a Bruker AC300 (75 MHz) spectrometer.

1,3,5-Tris(4-pyridylpyridiniummethyl)benzene tris(hexafluorophosphate) $2\cdot 3PF_6$

1,3,5-Tris(bromomethyl)benzene **1** (0.890 g, 2.50 mmol) was added as a solid portionwise over 24 h to a refluxing solution of 4,4'-bipyridine (11.47 g, 73.4 mmol) in dry MeCN (200 mL). The reaction mixture was heated under reflux for a further 3 d. After allowing it to cool down to room temperature, the reaction mixture was filtered and the solid residue was washed with MeCN (100 mL), followed by Et_2O (100 mL) and then dissolved in H_2O (400 mL). The resulting solution was filtered and then extracted with $CHCl_3$ (2 × 200 mL). The addition of a saturated aqueous solution of NH_4PF_6 to the aqueous layer afforded a precipitate, which was filtered off and purified by column chromatography [SiO_2, MeOH–NH_4Cl(2M)–$MeNO_2$, 7 : 2 : 1]. The resulting solid was dissolved in H_2O (200 mL) and a saturated solution of NH_4PF_6 was added to afford a white precipitate, which was filtered off to yield $\mathbf{2}\cdot 3PF_6$ (1.54 g, 61%): mp 240 °C (decomposition); LSI-MS: *m/z* 875 [M − PF_6]$^+$, 729 [M − $2PF_6$]$^+$; ^{1}H-NMR (CD_3COCD_3): δ 9.25 (6H, d, *J* = 7 Hz), 8.87–8.82 (6H, m), 8.60 (6H, d, *J* = 7 Hz), 8.09 (3H, s), 7.95–7.90 (6H, m), 6.17 (6H, m); ^{13}C-NMR (CD_3CN): δ 155.7, 152.1, 146.0, 141.8, 136.1, 131.9, 127.1, 122.6, 63.9. Anal. calcd for $C_{39}H_{33}F_{18}N_6P_3$: C 45.90, H 3.26, N 8.23; found C 46.00, H 3.27, N 8.44.

Hexakis(hexafluorophosphate) salt $4\cdot 6PF_6$

A solution of $\mathbf{2}\cdot 3PF_6$ (245 mg, 0.2 mmol) and the freshly prepared chloride **3** (1.400 g, 2.0 mmol) in dry DMF (10 mL) was subjected to a pressure of 15 kbar at 40 °C for 48 h. The solvent was removed *in vacuo* and the solid residue was washed with Et_2O (60 mL) before being dissolved in H_2O–$(Me)_2CO$ (1 : 1, v/v, 200 mL). An aqueous solution of NH_4PF_6 was added and, after the evaporation of Me_2CO, a white solid precipitated. The solid was filtered off, washed with H_2O (50 mL) and purified by column chromatography (SiO_2, 0.08 M NH_4PF_6 in Me_2CO) to yield $\mathbf{4}\cdot 6PF_6$ (372 mg, 47%): mp 225 °C (decomposition); ES-MS: *m/z* 2106 [2M − $3PF_6$]$^{3+}$, 1543 [M − $2PF_6$]$^{2+}$; ^{1}H-NMR (CD_3COCD_3): δ 9.42 (6H, d, *J* = 7 Hz), 9.26 (6H, d, *J* = 7 Hz), 8.69 (6H, d, *J* = 7 Hz), 8.64 (6H, d, *J* = 7 Hz), 8.04 (3H, s), 7.63 (6H, d, *J* = 9 Hz), 7.30 (12H, d, *J* = 9 Hz), 7.15–7.04 (36H, m), 6.83 (6H, d, *J* = 9 Hz), 6.14 (6H, s), 6.09 (6H, s), 4.23–4.17 (6H, m), 4.16–4.09 (6H, m), 3.93–3.64 (12H, m), 2.28 (9H, s), 1.29 (54H, s); ^{13}C-NMR (CD_3CN): δ 161.2, 157.7, 151.5, 151.2, 149.1, 146.7, 146.4, 145.3, 145.2, 140.3, 136.3, 135.9, 132.7, 132.1, 131.6, 131.3, 128.8, 128.4, 128.2, 125.7, 125.0, 116.3, 114.0, 70.4, 70.2, 68.5, 68.1, 65.4, 64.6, 63.9, 34.7, 31.6, 20.8. Anal. calcd for $C_{174}H_{186}F_{36}N_6O_9P_6\cdot 2H_2O$: C 61.92, H 5.55, N 2.49; found C 61.26, H 5.61, N 2.46.

[2]Rotaxane $5\cdot 6PF_6$, [3]rotaxane $6\cdot 6PF_6$, and [4]rotaxane $7\cdot 6PF_6$

Method A. A solution of $\mathbf{4}\cdot 6PF_6$ (169.0 mg, 0.05 mmol) and BPP34C10 (54.0 mg, 0.10 mmol) in dry MeCN (1.6 mL) was stirred at 50 °C for 10 d. The solvent was removed *in vacuo* and the solid residue was purified by preparative TLC [SiO_2, MeOH–CH_2Cl_2–$MeNO_2$–NH_4Cl(2 M), 140 : 32 : 18 : 10] to

give, after counter ion exchange (Me_2CO–H_2O, saturated aqueous solution of NH_4PF_6), in order of elution, the [4]rotaxane $\mathbf{7}\cdot 6PF_6$, [3]rotaxane $\mathbf{6}\cdot 6PF_6$ and a red solid, which was purified further by column chromatography [SiO_2, MeOH–CH_2Cl_2–NH_4Cl(2 M), 8 : 8 : 1.5] to give the [2]rotaxane $\mathbf{5}\cdot 6PF_6$, after counter ion exchange (Me_2CO–H_2O, saturated aqueous solution of NH_4PF_6). $\mathbf{5}\cdot 6PF_6$ (90.2 mg, 46%): mp 207 °C (decomposition); ES-MS: *m/z* 2464 $[2M - 3PF_6]^{3+}$, 1811 $[M - 2PF_6]^{2+}$; ^{1}H-NMR (CD_3COCD_3): δ 9.37 (4H, d, $J = 7$ Hz), 9.29 (4H, d, $J = 7$ Hz), 9.09 (2H, d, $J = 7$ Hz), 9.02 (2H, d, $J = 7$ Hz), 8.59 (4H, d, $J = 7$ Hz), 8.54 (4H, d, $J = 7$ Hz), 8.17–8.09 (7H, m), 7.69 (2H, d, $J = 9$ Hz), 7.62 (4H, d, $J = 9$ Hz), 7.32–7.27 (12H, m), 7.15–7.05 (36H, m), 6.87–6.76 (6H, m), 6.22 (4H, s), 6.16 (2H, s), 6.05 (4H, s), 5.99 (2H, s), 5.96 (8H, s), 4.25–4.17 (6H, m), 4.16–4.08 (6H, m), 3.93–3.85 (12H, m), 3.84–3.55 (32H, m), 2.28 (9H, s), 1.29 (54H, s); ^{13}C-NMR (CD_3CN): δ 161.3, 157.7, 152.8, 151.4, 149.5, 146.8, 146.7, 146.2, 145.6, 145.5, 140.7, 136.4, 135.9, 132.8, 132.5, 132.3, 131.5, 131.3, 129.2, 128.4, 128.1, 125.4, 116.5, 116.4, 115.7, 114.4, 71.3, 71.2, 70.6, 70.5, 70.3, 68.8, 68.4, 65.4, 64.9, 64.1, 35.0, 31.6, 29.7, 20.9. Anal. calcd for $C_{202}H_{226}F_{36}N_6O_{19}P_6$: C 62.02, H 5.82, N 2.15; found C 62.15, H 5.93, N 2.16. $\mathbf{6}\cdot 6PF_6$ (56.1 mg, 26%): mp 189 °C (decomposition); ES-MS: *m/z* 2821 $[2M - 3PF_6]^{3+}$, 2080 $[M - 2PF_6]^{2+}$, 1338 $[M - 3PF_6]^{3+}$; ^{1}H-NMR (CD_3COCD_3): δ 9.32 (2H, d, $J = 7$ Hz), 9.24 (2H, d, $J = 7$ Hz), 9.15 (4H, d, $J = 7$ Hz), 9.12 (4H, d, $J = 7$ Hz), 8.52 (2H, d, $J = 7$ Hz), 8.36 (2H, d, $J = 7$ Hz), 8.28–8.19 (8H, m), 8.11 (3H, s), 7.71 (4H, d, $J = 9$ Hz), 7.60 (2H, d, $J = 9$ Hz), 7.30 (12H, d, $J = 9$ Hz), 7.15–7.05 (36H, m), 6.82 (6H, d, $J = 9$ Hz), 6.27 (6H, s), 6.05 (16H, s), 6.02 (4H, s), 6.01 (2H, s), 4.25–4.17 (6H, m), 4.15–4.07 (6H, m), 3.92–3.84 (12H, m), 3.83–3.60 (64H, m), 2.28 (9H, s), 1.29 (54H, s); ^{13}C-NMR (CD_3CN): δ 161.3, 157.8, 153.1, 149.6, 147.7, 146.8, 146.5, 146.2, 145.7, 145.6, 140.9, 136.7, 136.5, 132.9, 132.6, 132.4, 131.7, 131.4, 129.3, 128.4, 128.1, 126.4, 126.1, 125.5, 116.6, 116.5, 115.9, 114.5, 71.5, 71.3, 70.8, 70.6, 70.5, 68.9, 68.6, 68.5, 65.1, 64.4, 64.2, 35.1, 31.7, 21.0. Anal. calcd for $C_{230}H_{266}F_{36}N_6O_{29}P_6$: C 62.10, H 6.03, N 1.89; found C 62.02, H 6.20, N 1.86. $\mathbf{7}\cdot 6PF_6$ (13.0 mg, 6%): mp 168 °C (decomposition); ES-MS: *m/z* 2348 $[M - 2PF_6]^{2+}$, 1517 $[M - 3PF_6]^{3+}$; ^{1}H-NMR (CD_3COCD_3): δ 9.20 (6H, d, $J = 7$ Hz), 9.11 (6H, d, $J = 7$ Hz), 8.31 (6H, d, $J = 7$ Hz), 8.27 (6H, d, $J = 7$ Hz), 8.12 (3H, s), 7.74 (6H, d, $J = 9$ Hz), 7.29 (12H, d, $J = 9$ Hz), 7.16–7.04 (36H, m), 6.82 (6H, d, $J = 9$ Hz), 6.33 (6H, s), 6.15 (24H, s), 6.06 (6H, s), 4.21 (6H, t, $J = 5$ Hz), 4.11 (6H, t, $J = 5$ Hz), 3.93–3.63 (108H, m), 2.28 (9H, s), 1.28 (54H, s); ^{13}C-NMR (CD_3CN): δ 161.2, 157.7, 153.0, 149.5, 146.8, 146.5, 145.6, 145.5, 140.7, 136.4, 132.8, 132.6, 131.5, 131.3, 129.2, 126.5, 126.1, 126.0, 125.6, 125.4, 116.4, 116.3, 115.8, 114.4, 71.3, 71.2, 70.7, 70.5, 70.3, 68.8, 68.6, 68.4, 65.1, 64.3, 64.1, 35.0, 31.6, 20.9; Anal. calcd for $C_{258}H_{306}F_{36}N_6O_{39}P_6$: C 62.16, H 6.19, N 1.68; C 62.10, H 6.56, N 1.73.

Method B. A solution of $\mathbf{4}\cdot 6PF_6$ (86.0 mg, 0.02 mmol) and BPP34C10 (175.0 mg, 0.30 mmol) in dry MeCN (1.6 mL) was stirred at 50 °C for 10 d. The solvent was removed *in vacuo* and the solid residue purified by preparative TLC [SiO_2, MeOH–CH_2Cl_2–$MeNO_2$–NH_4Cl(2 M), 140 : 32 : 18 : 10] to give, after counter ion exchange (Me_2CO–H_2O, saturated aqueous solution of NH_4PF_6), in order of elution, $\mathbf{7}\cdot 6PF_6$ (28.0 mg, 22%), $\mathbf{6}\cdot 6PF_6$ (45.3 mg, 41%), and a red solid, which was purified further by column chromatography [SiO_2, MeOH–CH_2Cl_2–NH_4Cl(2 M), 8 : 8 : 1.5], to afford $\mathbf{5}\cdot 6PF_6$ (17.2 mg, 19%), after counter ion exchange (Me_2CO–H_2O, saturated aqueous solution of NH_4PF_6).

Absorption and luminescence measurements

Room temperature experiments were carried out in MeCN solutions. Electronic absorption spectra were recorded with a Perkin-Elmer λ6 spectrophotometer, emission spectra with a Perkin-Elmer LS50 spectrofluorimeter. Fluorescence quantum yields were determined using naphthalene in degassed cyclohexane as a standard ($\Phi = 0.23$).[21] Lifetime measurements were performed with a previously described Edinburgh single-photon counting equipment.[22] Experimental errors: absorption maxima, ±2 nm; emission maxima, ±2 nm; excited-state lifetimes, ±10%; fluorescence quantum yields, ±20%.

Electrochemical measurements

Electrochemical experiments were carried out in argon-purged acetonitrile solution with a Princeton Applied Research 273 multipurpose instrument interfaced to a personal computer, using cyclic voltammetry (CV) and differential pulse voltammetry (DPV) techniques. The working electrode was a glassy carbon electrode (0.08 cm^2, Amel); its surface was routinely polished with a 0.05 μm alumina–water slurry on a felt surface immediately prior to use. The counter electrode was a Pt wire and the reference electrode was a saturated calomel electrode (SCE) separated with a fine glass frit. The concentration of the examined compounds was 5.0×10^{-4} M; 0.05 M tetraethylammonium hexafluorophosphate was added as supporting electrolyte. Cyclic voltammograms were obtained at sweep rates of 20, 50, 200 and 500 mV s^{-1}; DPV experiments were performed with a scan rate of 20 or 4 mV s^{-1}, a pulse height of 75 or 10 mV, and a duration of 40 ms. For reversible processes, the same halfwave potential values are obtained from the DPV peaks and from an average of the cathodic and anodic cyclic voltammetric peaks. For irreversible processes, the reported potential values are those evaluated from the DPV peaks. Both CV and DPV techniques have been used to measure the number of the exchanged electrons in each redox process;[23] since the results obtained for irreversible processes can be unreliable, no quantitative conclusions have been drawn on the number of electrons exchanged in the oxidation processes. To establish the reversibility of a process, we used the criteria of (*i*) separation of 60 mV between cathodic and anodic peaks, (*ii*) close to unity ratio of the intensities of the cathodic and anodic currents, and (*iii*) constancy of the peak potential on changing sweep rate in the cyclic voltammograms. The experimental error on the potential values was estimated to be ±10 mV.

Field-emission scanning electron microscopy

A solution of $\mathbf{4}\cdot 6PF_6$ in THF (100 μL) was dropped onto a glass plate. After the slow evaporation of the solvent, the plate was placed in a vacuum chamber equipped with a pair of planar electrodes. In order to render the surface of the sample conductive, OsO_4 was added into the chamber and polymerized by applying a direct current voltage of 1.0 kV. The resulting sample was analyzed by employing a TOPCON DS-720 field-emission scanning electron microscope (FE-SEM) with an acceleration voltage of 15 kV.

Molecular modeling

The rotaxanes were constructed within the input mode of Macromodel 5.0[15] and then the geometries were optimized by energy minimization performed employing the Polak–Ribiere conjugate gradient (PRCG) method[24] in conjunction with the AMBER* force field.[25] The resulting structures were subjected individually to simulated annealing performed employing the AMBER* force field, the generalized-Born surface area (GB/SA) solvation model[26] for H_2O, and the PRCG minimization algorithm. The temperature was gradually decreased from 500 to 50 K in ten consecutive molecular dynamics steps of 20.0 ps each. The bath constant and the time-step were mantained at 5.0 ps and 1.5 fs, respectively, in all steps. The dimeric aggregate of the triply branched compound $\mathbf{4}^{6+}$ was

constructed within the input mode of Macromodel 5.0 and the geometry was optimized by PRCG minimization performed employing the AMBER* force field. The resulting structure was subjected to simulated annealing performed as described for the rotaxanes in conjunction with the GB/SA solvation model for either $CHCl_3$ or H_2O.

Surface-pressure–area measurements

Surface-pressure–area isotherms were measured with a Langmuir film balance (Nippon Laser & Electronics Lab., NL-LB-240-MWC). A Teflon trough was filled with Milli-Q treated and doubly distilled H_2O and spectroscopic grade THF was used as the spreading solvent. A measured amount of a solution of the compound (0.2 mg mL^{-1}) was delivered to the H_2O surface by employing a microsyringe. The temperature of the subphase was maintained at 25 °C and the surface pressure was increased to the desired value and maintained constant while the surface area changes were recorded continuously. The microscopic observation of the monolayers at the air–water interface was carried out with a Brewster angle microscope (Nippon Laser & Electronic Lab., NL-EMM633). This microscopic technique is essentially an ellipsometry[27] and hence a monolayer image arises from the refractive index difference between the monolayer and the subphase.

Atomic force microscopy

The shape of the monolayers were observed with an atomic force microscope (Digital Instruments, Inc., Nanoscope IIIa) in the tapping mode.[28] The monolayers were transferred onto freshly cleaved mica by a horizontal lifting method while the surface pressure was maintained at 15 or 30 mN m^{-1}: the transfer ratios were 1.0–1.2. Atomic force images were produced in the 'height' mode using Nanoscope silicon cantilevers (125 mm, tip radius 5–10 mm) at a scan speed of 1 mm s^{-1}.

Acknowledgements

This research was supported by the Engineering and Physical Sciences Research Council, the European Community Human Capital and Mobility Programme, and the North Atlantic Treaty Organization (Collaborative Research Grant No. 960659) in the UK, the University of Bologna (Funds for Selected Research Topics) and CNR (Progetto Strategico Tecnologie Chimiche Innovative) in Italy, and the EU TMR grant FMRX-CT96-0076.

References

1 Part 35: P. R. Ashton, V. Balzani, A. Credi, O. Kocian, D. Pasini, L. Prodi, N. Spencer, J. F. Stoddart, M. S. Tolley, M. Venturi, A. J. P. White and D. J. Williams, *Chem. Eur. J.*, 1998, **4**, 590.

2 (*a*) G. Schill, *Catenanes, Rotaxanes and Knots*, Academic Press, New York, 1971; (*b*) D. M. Walba, *Tetrahedron*, 1985, **41**, 3161; (*c*) C. O. Dietrich-Buchecker and J.-P. Sauvage, *Chem. Rev.*, 1987, **87**, 795; (*d*) Y. S. Lipatov, T. E. Lipatova and L. F. Kosyanchuk, *Adv. Polym. Sci.*, 1989, **88**, 49; (*e*) C. O. Dietrich-Buchecker and J.-P. Sauvage, *Bioorg. Chem. Front.*, 1991, **2**, 195; (*f*) H. W. Gibson and H. Marand, *Adv. Mater.*, 1993, **5**, 11; (*g*) J.-C. Chambron, C. O. Dietrich-Buchecker and J.-P. Sauvage, *Top. Curr. Chem.*, 1993, **165**, 131; (*h*) H. W. Gibson, M. C. Bheda and P. T. Engen, *Prog. Polym. Sci.*, 1994, **19**, 843; (*i*) D. B. Amabilino, I. W. Parsons and J. F. Stoddart, *Trends Polym. Sci.*, 1994, **2**, 146; (*j*) D. B. Amabilino and J. F. Stoddart, *Chem. Rev.*, 1995, **95**, 2725; (*k*) M. Belohradsky, F. M. Raymo and J. F. Stoddart, *Collect. Czech. Chem. Commun.*, 1996, **61**, 1; (*l*) T. Dünnwald, R. Jäger and F. Vögtle, *Chem. Eur. J.*, 1997, **3**, 2043.

3 (*a*) M. Born and H. Ritter, *Makromol. Chem., Rapid Commun.*, 1991, **12**, 471; (*b*) H. Ritter, *Am. Chem. Soc., Div. Polym. Chem., Polym. Prepr.*, 1993, **34**(1), 66; (*c*) H. Ritter, *Macromol. Symp.*, 1994, **77**, 73; (*d*) M. Born and H. Ritter, *Angew. Chem., Int. Ed. Engl.*, 1995, **34**, 309; (*e*) M. Born and H. Ritter, *Adv. Mater.*, 1996, **8**, 149.

4 (*a*) D. A. Tomalia, A. M. Naylor and W. A. Goddard III, *Angew. Chem., Int. Ed. Engl.*, 1990, **29**, 138; (*b*) Y. H. Kim, *Adv. Mater.*, 1992, **4**, 764; (*c*) G. R. Newkome, C. N. Moorefield and R. Baker, *Aldrichimica Acta*, 1992, **25**, 31; (*d*) H. B. Mekelburger, W. Jaworek and F. Vögtle, *Angew. Chem., Int. Ed. Engl.*, 1992, **31**, 1571; (*e*) A. W. van der Made, P. W. N. M. van Leeuwen, J. C. de Wielde and R. Brandes, *Adv. Mater.*, 1993, **5**, 466; (*f*) D. A. Tomalia, *Aldrichimica Acta*, 1993, **26**, 91; (*g*) D. A. Tomalia and H. D. Durst, *Top. Curr. Chem.*, 1993, **165**, 193; (*h*) D. A. Tomalia, *Adv. Mater.*, 1994, **6**, 529; (*i*) A. Rajca, *Adv. Mater.*, 1994, **6**, 605; (*j*) J. Issberner, R. Moors and F. Vögtle, *Angew. Chem., Int. Ed. Engl.*, 1994, **33**, 2413; (*k*) H. W. Gibson, *Nature* (*London*), 1994, **371**, 106; (*l*) D. A. Tomalia and P. R. Dvornic, *Nature* (*London*), 1994, **372**, 617; (*m*) J. M. J. Fréchet, *Science*, 1994, **263**, 1710; (*n*) D. A. Tomalia, *Sci. Am.*, 1995, **272**(5), 62; (*o*) G. R. Newkome, C. N. Moorefield and F. Vögtle, *Dendritic Macromolecules*, VCH, Weinheim, 1996; (*p*) J. F. Labarre, F. Crasnier and F. Sournies, *Synlett*, 1996, 799; (*q*) M. Johansson, E. Malmström and E. Hult, *Trends Polym. Sci.*, 1996, **4**, 398; (*r*) E. C. Constable, *Chem. Commun.*, 1997, 1073; (*s*) F. Zeng and S. C. Zimmerman, *Chem. Rev.*, 1997, **97**, 1681; (*t*) S. Mukamel, *Nature* (*London*), 1997, **388**, 425; (*u*) H. F. Chow and C. C. Mak, *Pure Appl. Chem.*, 1997, **69**, 483; (*v*) O. A. Matthews, A. N. Shipway and J. F. Stoddart, *Prog. Polym. Sci.*, 1998, **23**, 1.

5 (*a*) P. R. Ashton, M. Belohradsky, D. Philp and J. F. Stoddart, *J. Chem. Soc., Chem. Commun.*, 1993, 1269; (*b*) P. R. Ashton, M. Belohradsky, D. Philp, N. Spencer and J. F. Stoddart, *J. Chem. Soc., Chem. Commun.*, 1993, 1274; (*c*) M. Belohradsky, D. Philp, F. M. Raymo and J. F. Stoddart, in *Organic Reactivity: Physical and Biological Aspects*, eds. B. T. Golding, R. J. Griffin and H. Maskill, RSC Special Publication No. 148, Cambridge, 1995, pp. 387–398; (*d*) D. B. Amabilino, P. R. Ashton, M. Belohradsky and F. M. Raymo, J. F. Stoddart, *J. Chem. Soc., Chem. Commun.*, 1995, 747; (*e*) D. B. Amabilino, P. R. Ashton, M. Belohradsky, F. M. Raymo and J. F. Stoddart, *J. Chem. Soc., Chem. Commun.*, 1995, 751; (*f*) P. R. Ashton, R. Ballardini, V. Balzani, M. Belohradsky, M. T. Gandolfi, D. Philp, L. Prodi, F. M. Raymo, M. V. Reddington, N. Spencer, J. F. Stoddart, M. Venturi and D. J. Williams, *J. Am. Chem. Soc.*, 1996, **118**, 4931; (*g*) M. Asakawa, P. R. Ashton, R. Ballardini, V. Balzani, M. Belohradsky, M. T. Gandolfi, O. Kocian, L. Prodi, F. M. Raymo, J. F. Stoddart and M. Venturi, *J. Am. Chem. Soc.*, 1997, **119**, 302; (*h*) F. M. Raymo and J. F. Stoddart, *Pure Appl. Chem.*, 1997, **69**, 1987.

6 (*a*) J. F. Stoddart, *Chirality in Drug Design and Synthesis*, ed. C. Brown, Academic Press, London, 1990, pp. 53–81; (*b*) T. E. Mallouk and H. Lee, *J. Chem. Educ.*, 1990, **67**, 829; (*c*) E. C. Constable, *Angew. Chem., Int. Ed. Engl.*, 1991, **30**, 1450; (*d*) J. S. Lindsey, *New J. Chem.*, 1991, **15**, 153; (*e*) G. M. Whitesides, J. P. Mathias and C. T. Seto, *Science*, 1991, **254**, 1312; (*f*) G. M. Whitesides, E. E. Simanek, J. P. Mathias, C. T. Seto, D. N. Chin, M. Mammen and D. M. Gordon, *Acc. Chem. Res.*, 1995, **25**, 37; (*g*) F. M. Menger, S. S. Lee and X. Tao, *Adv. Mater.*, 1995, **7**, 669; (*h*) M. R. Ghadiri, *Adv. Mater.*, 1995, **7**, 675; (*i*) C. A. Hunter, *Angew. Chem., Int. Ed. Engl.*, 1995, **34**, 1079; (*j*) D. S. Lawrence, T. Jiang and M. Levett, *Chem. Rev.*, 1995, **95**, 2229; (*k*) D. Philp and J. F. Stoddart, *Angew. Chem., Int. Ed. Engl.*, 1996, **35**, 1154; (*l*) F. M. Raymo and J. F. Stoddart, *Curr. Opin. Coll. Interf. Sci.*, 1996, **1**, 116; (*m*) M. C. T. Fyfe and J. F. Stoddart, *Acc. Chem. Res.*, 1997, **30**, 393.

7 (*a*) M. H. Schwartz, *J. Incl. Phenom.*, 1990, **9**, 1; (*b*) C. A. Hunter and J. K. M. Sanders, *J. Am. Chem. Soc.*, 1990, **112**, 5525; (*c*) H.-J. Schneider, *Angew. Chem., Int. Ed. Engl.*, 1991, **30**, 1417; (*d*) F. Cozzi, M. Cinquini, R. Annunziata, T. Dwyer and J. S. Siegel, *J. Am. Chem. Soc.*, 1992, **114**, 5729; (*e*) J. H. Williams, *Acc. Chem. Res.*, 1993, **26**, 593; (*f*) C. A. Hunter, *Angew. Chem., Int. Ed. Engl.*, 1993, **32**, 1584; (*g*) F. Cozzi, M. Cinquini, R. Annunziata and J. S. Siegel, *J. Am. Chem. Soc.*, 1993, **115**, 5330; (*h*) C. A. Hunter, *J. Mol. Biol.*, 1993, **230**, 1025; (*i*) T. Dahl, *Acta Chem. Scand.*, 1994, **48**, 95; (*j*) F. Cozzi and J. S. Siegel, *Pure Appl. Chem.*, 1995, **67**, 683; (*k*) A. S. Shetty, J. Zhang and J. S. Moore, *J. Am. Chem. Soc.*, 1996, **118**, 1019.

8 (*a*) M. Etter, *Acc. Chem. Res.*, 1990, **23**, 120; (*b*) M. C. Etter, J. C. MacDonald and J. Bernstein, *Acta Crystallogr., Sect. B*, 1990, **46**, 256; (*c*) J. Rebek, Jr., *Angew. Chem., Int. Ed. Engl.*, 1990, **29**, 245; (*d*) A. D. Hamilton, *J. Chem. Educ.*, 1990, **67**, 821; (*e*) G. R. Desiraju, *Acc. Chem. Res.*, 1991, **24**, 290; (*f*) C. B. Aakeröy and K. R. Seddon, *Chem. Soc. Rev.*, 1993, **22**, 397; (*g*) J. C. MacDonald and G. M. Whitesides, *Chem. Rev.*, 1994, **94**, 2383; (*h*) J.-M. Lehn, *Pure Appl. Chem.*, 1994, **66**, 1961; (*i*) J. Bernstein, R. E. Davis, L. Shimoni and N. L. Chang, *Angew. Chem., Int. Ed. Engl.*, 1995, **34**, 1555; (*j*) A. D. Burrows, C. W. Chan, M. M. Chowdhry, J. E. McGrady and D. M. P. Mingos, *Chem. Soc. Rev.*, 1995, **24**, 329; (*k*) J. A. Platts, S. T. Howard and B. R. F. Bracke, *J. Am. Chem. Soc.*, 1996, **118**, 2726; (*l*) G. R. Desiraju, *Chem. Commun.*, 1997, 1475; (*m*) G. R. Desiraju, *Curr. Opin. Solid State Mater. Sci.*, 1997, **2**, 451.

9 A similar result was observed in the case of [2]- and [3]-catenanes incorporating bipyridinium-based and hydroquinone-based macrocyclic components. See: P. R. Ashton, C. L. Brown, J. R. Chapman, R. T. Gallagher and J. F. Stoddart, *Tetrahedron Lett*., 1992, **33**, 7771.
10 Kinetic studies on the slippage approach to linear rotaxanes [refs. 5(h), (i)] demonstrated that low values of the free energies of activation are associated with the slipping-on and -off of the macrocyclic component over the stoppers of the dumbbell-shaped component in $CHCl_3$—*i.e*., the rotaxane along with the 'free' macrocyclic and the dumbbell-shaped components are in fast exchange. As a result of their low kinetic stabilities, the potential aggregation of the branched [*n*]rotaxanes in $CHCl_3$ could not be investigated.
11 P.-L. Anelli, P. R. Ashton, R. Ballardini, V. Balzani, M. Delgado, M. T. Gandolfi, T. T. Goodnow, A. E. Kaifer, D. Philp, M. Pietraszkiewicz, L. Prodi, M. V. Reddington, A. M. Z. Slawin, N. Spencer, J. F. Stoddart, C. Vincent and D. J. Williams, *J. Am. Chem. Soc*., 1992, **114**, 193.
12 D. B. Amabilino, P. R. Ashton, V. Balzani, C. L. Brown, A. Credi, J. M. J. Fréchet, J. W. Leon, F. M. Raymo, N. Spencer, J. F. Stoddart and M. Venturi, *J. Am. Chem. Soc*., 1996, **118**, 12012.
13 E. P. Parry and R. A. Osteryoung, *Anal. Chem*., 1965, **37**, 1634.
14 The small shift of this wave toward more negative potentials compared with the reduction of $\mathbf{4}^{6+}$ is consistent with the possibility that the bipyridinium units not encircled by a crown ether can be engaged in alongside donor–acceptor interactions with the crown ether encircling another bipyridinium unit.
15 F. Mohamadi, N. G. J. Richards, W. C. Guida, R. Liskamp, M. Lipton, C. Caufield, G. Chang, T. Hendrickson and W. C. Still, *J. Comput. Chem*., 1990, **11**, 440.
16 In Macromodel 5.0, negative charges can be located on oxygen and/or sulfur atoms only. As a result, acetate instead of hexafluorophosphate counter ions were employed.
17 For examples of Langmuir films generated with bipyridinium-based compounds, see: (*a*) R. C. Ahuja, P.-L. Caruso, D. Möbius, G. Wildburg, H. Ringsdorf, D. Philp, J. A. Preece and J. F. Stoddart, *Langmuir*, 1993, **9**, 1534; (*b*) R. C. Ahuja, P.-L. Caruso, D. Möbius, G. Wildburg, H. Ringsdorf, D. Philp, J. A. Preece and J. F. Stoddart, *Thin Solid Films*, 1996, **284**/**285**, 671.
18 (*a*) V. Balzani and F. Scandola, *Supramolecular Photochemistry*, Ellis Horwood, Chichester, 1991; (*b*) J.-M. Lehn, *Supramolecular Chemistry*, VCH, Weinheim, 1995; (*c*) P. D. Beer, *Adv. Inorg. Chem*., 1992, **39**, 79; (*d*) R. A. Bissell, A. P. de Silva, H. Q. N. Gunaratne, P. L. M. Lynch, G. E. M. Maguire, C. P. McCoy and K. R. A. S. Sandanayake, *Top. Curr. Chem*., 1993, **168**, 223; (*e*) A. W. Czarnik, *Acc. Chem. Res*., 1994, **27**, 302; (*f*) L. Fabbrizzi and A. Poggi, *Chem. Soc. Rev*., 1995, **24**, 197; (*g*) V. Balzani, A. Juris, M. Venturi, S. Campagna and S. Serroni, *Chem. Rev*. 1996, **96**, 759; (*h*) for recent examples of molecular machines, see: P. R. Ashton, R. Ballardini, V. Balzani, S. E. Boyd, A Credi, M. T. Gandolfi, M. Gómez-López, S. Iqbal, D. Philp, J. A. Preece, L. Prodi, H. G. Ricketts, J. F. Stoddart, M. S. Tolley, M. Venturi, A. J. P. White and D. J. Williams, *Chem. Eur. J*., 1997, **3**, 152, and references therein.
19 B. S. Furniss, A. J. Hannaford, P. W. G. Smith and A. R. Tatchell, *Practical Organic Chemistry*, Longman, New York, 1989.
20 F. Vögtle, M. Zuber and R. G. Lichtenthaler, *Chem. Ber*., 1973, **106**, 717.
21 I. B. Berlman, *Handbook of Fluorescence Spectra of Aromatic Compounds*, Academic Press, London, 1965.
22 N. Armaroli, V. Balzani, F. Barigelletti, L. De Cola, L. Flamigni, J.-P. Sauvage and C. Hemmert, *J. Am. Chem. Soc*., 1994, **116**, 5211.
23 J. B. Flanagan, S. Margel, A. J. Bard and F. C. Anson, *J. Am. Chem. Soc*., 1978, **100**, 4248.
24 E. Polak and G. Ribiere, *Revue Francaise Inf. Rech. Oper*., 1969, **16-R1**, 35.
25 S. J. Weiner, P. A. Kollman, D. A. Case, V. C. Singh, C. Ghio, G. Alagona, S. Profeta, Jr and P. Weiner, *J. Am. Chem. Soc*., 1984, **106**, 765.
26 W. C. Still, A. Tempczyk, R. C. Hawley and T. Hendrickson, *J. Am. Chem. Soc*., 1990, **112**, 6127.
27 (*a*) S. Henon and J. Meunier, *Rev. Sci. Instrum*., 1991, **62**, 936; (*b*) D. Hoig and D. Hoius, *J. Phys. Chem*., 1991, **95**, 4590.
28 L. D. Martin, J. P. Vesenka, E. Henderson and D. L. Dobbs, *Biochemistry*, 1993, **34**, 8390.

Received in Cambridge, UK, 14*th April* 1998;
Paper 8/02784F